

1 **High organic inputs explain shallow and deep SOC storage in a long-term agroforestry**
2 **system – Combining experimental and modeling approaches.**

3

4 Rémi Cardinael^{a,b,c,d*}, Bertrand Guenet^e, Tiphaine Chevallier^a, Christian Dupraz^f, Thomas
5 Cozzi^b, Claire Chenu^b

6

7 ^a Eco&Sols, IRD, CIRAD, INRA, Montpellier SupAgro, Univ Montpellier, Montpellier, France

8 ^b AgroParisTech, UMR Ecosys, Avenue Lucien Brétignières, 78850 Thiverval-Grignon, France

9 ^c CIRAD, UPR AIDA, F-34398 Montpellier, France (present address)

10 ^d AIDA, Univ Montpellier, CIRAD, Montpellier, France

11 ^e Laboratoire des Sciences du Climat et de l'Environnement, UMR CEA-CNRS-UVSQ, CE

12 L'Orme des Merisiers, 91191 Gif-Sur-Yvette, France

13 ^f System, INRA, CIRAD, Montpellier SupAgro, Univ Montpellier, Montpellier, France

14 * Corresponding author. Tel.: +33 04.67.61.53.08. E-mail address: remi.cardinael@cirad.fr

15

16 *Keywords:* priming effect, deep roots, deep soil organic carbon, spatial heterogeneity,
17 silvoarable system, crop yield, SOC modeling

18

19 **Abstract**

20 Agroforestry is an increasingly popular farming system enabling agricultural diversification

21 and providing several ecosystem services. In agroforestry systems, soil organic carbon (SOC)

22 stocks are generally increased, but it is difficult to disentangle the different factors responsible

23 for this storage. Organic carbon (OC) inputs to the soil may be larger, but SOC decomposition

24 rates may be modified owing to microclimate, physical protection, or priming effect from roots,

25 especially at depth. We used an 18-year-old silvoarable system associating hybrid walnut trees

26 (*Juglans regia* × *nigra*) and durum wheat (*Triticum turgidum* L. subsp. *durum*), and an adjacent
27 agricultural control plot to quantify all OC inputs to the soil - leaf litter, tree fine root
28 senescence, crop residues, and tree row herbaceous vegetation -, and measure SOC stocks down
29 2 m depth at varying distances from the trees. We then proposed a model that simulates SOC
30 dynamics in agroforestry accounting for both the whole soil profile and the lateral spatial
31 heterogeneity. The model was calibrated to the control plot only.
32 Measured OC inputs to soil were increased by about 40% (+ 1.11 t C ha⁻¹ yr⁻¹) down to 2 m
33 depth in the agroforestry plot compared to the control, resulting in an additional SOC stock of
34 6.3 t C ha⁻¹ down to 1 m depth. However, most of the SOC storage occurred in the first 30 cm
35 of soil and in the tree rows. The model was strongly validated, describing properly the measured
36 SOC stocks and distribution with depth in agroforestry tree rows and alleys. It showed that the
37 increased inputs of fresh biomass to soil explained the observed additional SOC storage in the
38 agroforestry plot. Moreover, only a priming effect variant of the model was able to capture the
39 depth distribution of SOC stocks, suggesting priming effect as a possible mechanism driving
40 deep SOC dynamics. This result questions the potential of soils to store large amounts of
41 carbon, especially at depth. Deep-rooted trees modify OC inputs to soil, a process that deserves
42 further studies given its potential effects on SOC dynamics.

43

44 **1 Introduction**

45 Agroforestry systems are complex agroecosystems combining trees and crops or pastures
46 within the same field (Nair, 1993, 1985; Somarriba, 1992). More precisely, silvoarable systems
47 associate parallel tree rows with annual crops. Some studies showed that these systems could
48 be very productive, with a land equivalent ratio (Mead and Willey, 1980) reaching up to 1.3
49 (Graves et al., 2007). Silvoarable systems may therefore produce up to 30% more marketable
50 biomass on the same area of land compared to crops and trees grown separately. This

51 performance can be explained by a better use of water, nutrients and light by the agroecosystem
52 throughout the year. Trees grown in silvoarable systems usually grow faster than the same trees
53 grown in forest ecosystems, because of their lower density, and because they also benefit from
54 the crop fertilization (Balandier and Dupraz, 1999; Chaudhry et al., 2003; Chiffot et al., 2006).
55 In temperate regions, farmers usually grow one crop per year, and this association of trees can
56 extend the growing period at the field scale, especially when winter crops are intercropped with
57 trees having a late bud break (Burgess et al., 2004). However, after several years, a decrease of
58 crop yield can be observed in mature and highly dense plantations, especially close to the trees,
59 due to competition between crops and trees for light, water, and nutrients (Burgess et al., 2004;
60 Dufour et al., 2013; Yin and He, 1997).

61 Part of the additional biomass produced in agroforestry is used for economical purposes, such
62 as timber or fruit production. Leaves, tree fine roots, pruning residues and the herbaceous
63 vegetation growing in the tree rows will usually return to the soil, contributing to a higher input
64 of organic carbon (OC) to the soil compared to an agricultural field (Peichl et al., 2006).

65 In such systems, the observed soil organic carbon (SOC) stocks are also generally higher
66 compared to a cropland (Albrecht and Kandji, 2003; Kim et al., 2016; Lorenz and Lal, 2014).
67 Cardinael *et al.*, (2017) measured a mean SOC stock accumulation rate of 0.24 (0.09-0.46) t C
68 ha⁻¹ yr⁻¹ at 0-30 cm depth in several silvoarable systems compared to agricultural plots in
69 France. Higher SOC stocks were also found in Canadian agroforestry systems, but measured
70 only to 20 cm depth (Bambrick et al., 2010; Oelbermann et al., 2004; Peichl et al., 2006).

71 To our knowledge, we are still not able to disentangle the factors responsible for such a higher
72 SOC storage. This SOC storage might be due to higher OC inputs but it could also be favored
73 by a modification of the SOC decomposition owing to a change in SOC physical protection
74 (Haile et al., 2010), and/or in soil temperature and moisture.

75 The introduction of trees in an agricultural field modifies the amount, but also the distribution
76 of fresh organic carbon (FOC) input to the soil, both vertically and horizontally (Bambrick et
77 al., 2010; Howlett et al., 2011; Peichl et al., 2006). FOC inputs from the trees decrease with
78 increasing distance from the trunk and with soil depth (Moreno et al., 2005). On the contrary,
79 crop yield usually increases with increasing distance from the trees (Dufour et al., 2013; Li et
80 al., 2008). Therefore, the proportions of FOC coming from both the crop residues and the trees
81 change with distance from the trees, soil depth, and time.

82 Tree fine roots (diameter ≤ 2 mm) are the most active part of root systems (Eissenstat and Yanai,
83 1997) and play a major role in carbon cycling. In silvoarable systems, tree fine root distribution
84 within the soil profile is strongly modified due to the competition with the crop, inducing a
85 deeper rooting compared to trees grown in forest ecosystems (Cardinael et al., 2015a; Mulia
86 and Dupraz, 2006). Deep soil layers may therefore receive significant OC inputs from fine root
87 mortality and exudates. Root carbon has a higher mean residence time in the soil compared to
88 shoot carbon (Kätterer et al., 2011; Rasse et al., 2006), presumably because root residues are
89 preferentially stabilized within microaggregates or adsorbed to clay particles. Moreover,
90 temperature and moisture conditions are more buffered in the subsoil than in the topsoil. The
91 microbial biomass is also smaller at depth (Eilers et al., 2012; Fierer et al., 2003), and the spatial
92 segregation with organic matter is larger (Salomé et al., 2010) resulting in lower decomposition
93 rates. Deep root carbon input in the soil could therefore contribute to a SOC storage with high
94 mean residence times. However, some studies showed that adding FOC – a source of energy
95 for microorganisms - to the subsoil enhanced decomposition of stabilized carbon, a process
96 called « priming effect » (Fontaine et al., 2007). The priming effect is stronger when induced
97 by labile molecules like root exudates than by root litter coming from the decomposition of
98 dead roots (Shahzad et al., 2015). Therefore, the net effect of deep roots on SOC stocks has to
99 be assessed, especially in silvoarable systems.

100 Models are crucial as they allow virtual experiments to best design and understand complex
101 processes in these systems (Luedeling et al., 2016). Several models have been developed to
102 simulate interactions for light, water and nutrients between trees and crops (Charbonnier et al.,
103 2013; Duursma and Medlyn, 2012; van Noordwijk and Lusiana, 1999; Talbot, 2011) or to
104 predict tree growth and crop yield in agroforestry systems (Graves et al., 2010; van der Werf et
105 al., 2007). However, none of these models are designed to simulate SOC dynamics in
106 agroforestry systems and they are therefore not useful to estimate SOC storage. Oelbermann &
107 Voroney (2011) evaluated the ability of the CENTURY model (Parton et al., 1987) to predict
108 SOC stocks in tropical and temperate agroforestry systems, but with a single-layer modeling
109 approach (0-20 cm). The approach of modeling a single topsoil layer assumes that deep SOC
110 does not play an active role in carbon cycling, while it was shown that deep soil layers contain
111 important amounts of SOC (Jobbagy and Jackson, 2000), and that part of this deep SOC could
112 cycle on decadal timescales due to root inputs or to dissolved organic carbon transport (Baisden
113 and Parfitt, 2007; Koarashi et al., 2012). The need to take into account deep soil layers when
114 modeling SOC dynamics is now well recognized in the scientific community (Baisden et al.,
115 2002; Elzein and Balesdent, 1995), and several models have been proposed (Braakhekke et al.,
116 2011; Guenet et al., 2013; Koven et al., 2013; Taghizadeh-Toosi et al., 2014; Ahrens et al.,
117 2015). Using vertically discretized soils is particularly important when modeling the impact of
118 agroforestry systems on SOC stocks, but to our knowledge, vertically spatialized SOC models
119 have not yet been tested for these systems.

120

121 The aims of this study were then twofold: (i) to propose a model of soil C dynamics in
122 agroforestry systems able to account for both vertical and lateral spatial heterogeneities and (ii)
123 to test whether variations of fresh organic carbon (FOC) input could explain increased SOC
124 stocks both using experimental data and model runs.

125 For this, we first compiled data on FOC inputs to the soil obtained in a 18-year-old agroforestry
126 plot and in an agricultural control plot in southern France, in which SOC stocks have been
127 recently quantified to 2 m depth (Cardinael et al., 2015b). FOC inputs comprised tree fine roots,
128 tree leaf litter, aboveground and belowground biomass of the crop and of the herbaceous
129 vegetation in the tree rows. We compiled recently published data for FOC inputs (Cardinael et
130 al., 2015a; Germon et al., 2016), and measured the others (Table 1).

131

132 We then modified a two pools model proposed by Guenet *et al.*, (2013), to create a spatialized
133 model over depth and distance from the tree, the CARBOSAF model (soil organic CARBOn
134 dynamics in Silvoarable AgroForestry systems). Based on data acquired since the tree planting
135 in 1995 (crop yield, tree growth), and on FOC inputs, we modeled SOC dynamics to 2 m depth
136 in both the silvoarable and agricultural control plot. We evaluated the model against measured
137 SOC stocks along the profile and used this opportunity to test the importance of priming effect
138 (*PE*) for deep soil C dynamics in a silvoarable system. The performance of the two pools model
139 including *PE* was also compared with a model version including three OC pools.

140

141 **2 Materials and methods**

142 **2.1 Study site**

143 The experimental site is located at the Restinclières farm Estate in Prades-le-Lez, 15 km North
144 of Montpellier, France (longitude 04°01' E, latitude 43°43' N, elevation 54 m a.s.l.). The
145 climate is sub-humid Mediterranean with an average temperature of 15.4°C and an average
146 annual rainfall of 973 mm (years 1995–2013). The soil is a silty and carbonated (pH = 8.2) deep
147 alluvial Fluvisol (IUSS Working Group WRB, 2007). In February 1995, a 4.6 hectare
148 silvoarable agroforestry plot was established with the planting of hybrid walnut trees (*Juglans*
149 *regia* × *nigra* cv. NG23) at a density of 192 trees ha⁻¹ but later thinned to 110 trees ha⁻¹. Trees

150 were planted at 13 m × 4 m spacing, and tree rows are East–West oriented. The cultivated alleys
 151 are 11 m wide. The remaining part of the plot (1.4 ha) was kept as an agricultural control plot.
 152 Since the tree planting, the agroforestry alleys and the control plot were managed in the same
 153 way. The associated crop is most of the time durum wheat (*Triticum turgidum* L. subsp. *durum*),
 154 except in 1998, 2001 and 2006, when rapeseed (*Brassica napus* L.) was cultivated, and in 2010
 155 and 2013, when pea (*Pisum sativum* L.) was cultivated. The soil is ploughed to a depth of 0.2
 156 m before sowing, and the wheat crop is fertilized with an average of 120 kg N ha⁻¹ yr⁻¹. Crop
 157 residues (wheat straw) are also exported, but about 25% remain on the soil. Tree rows are
 158 covered by spontaneous herbaceous vegetation. Two successive herbaceous vegetation types
 159 occur during the year, one in summer and one in winter. The summer vegetation is mainly
 160 composed of *Avena fatua* L., and is 1.5 m tall. In winter, the vegetation is a mix of *Achillea*
 161 *millefolium* L., *Galium aparine* L., *Vicia* L., *Ornithogalum umbellatum* L. and *Avena fatua* L.,
 162 and is 0.2 m tall.

163

164 **Table 1.** Synthesis of the different field and laboratory data available or measured, and their
 165 sources.

Description of the data	Source
Soil texture, bulk densities, SOC stocks	Cardinael <i>et al.</i> , (2015a)
Soil temperature and soil moisture	Measured
Tree growth (DBH)	Measured
Tree wood density	(Talbot, 2011)
Tree fine root biomass	Cardinael <i>et al.</i> , (2015b)
Tree fine root turnover	Germon <i>et al.</i> , (2016)
Crop yield and crop ABG biomass	Dufour <i>et al.</i> , (2013) and measured
Crop root biomass	Prieto <i>et al.</i> , (2015) and measured
Tree row herbaceous vegetation – ABG biomass	Measured
Tree row herbaceous vegetation – root biomass	Measured
Biomass carbon concentrations	Measured
Potential decomposition rate of roots	Prieto <i>et al.</i> , (2016a)
HSOC potential decomposition rate	Measured

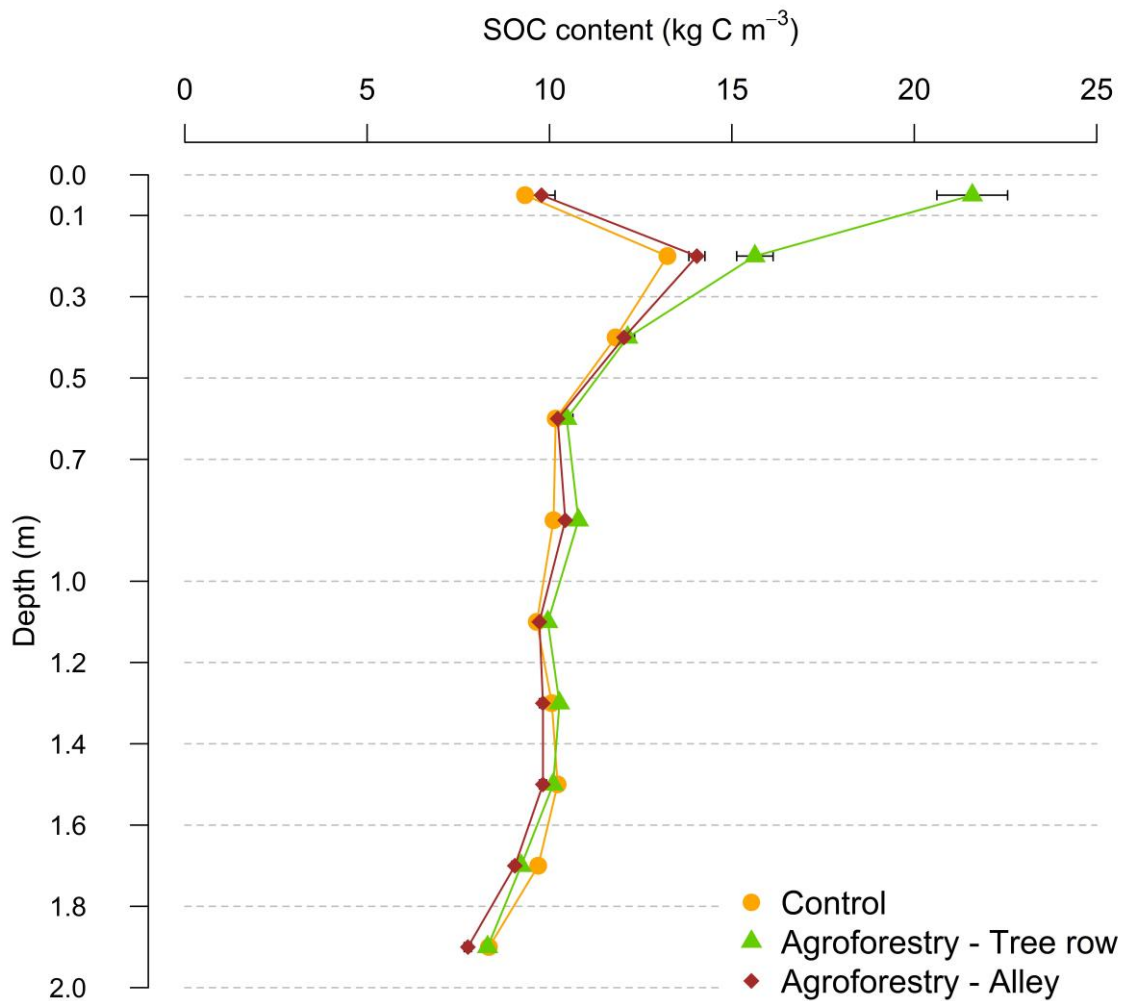
166 DBH: Diameter at Breast Height; ABG: aboveground; OC: organic carbon; HSOC: humified
 167 soil organic carbon.

168

169 2.2 Organic carbon stocks

170 2.2.1 Soil organic carbon stocks

171 SOC data have been published in Cardinael *et al.*, (2015b) (Fig. 1). Briefly, soil cores were
172 sampled down to 2 m depth in May 2013, 100 in the agroforestry plot, and 93 in the agricultural
173 control plot. SOC concentrations, soil bulk densities, SOC stocks, and soil texture were
174 measured for ten soil layers (0.0-0.1, 0.1-0.3, 0.3-0.5, 0.5-0.7, 0.7-1.0, 1.0-1.2, 1.2-1.4, 1.4-1.6,
175 1.6-1.8, and 1.8-2.0 m). In the agroforestry plot, 40 soil cores were taken in the tree rows, while
176 60 were sampled in the alleys at varying distances from the trees. Soil organic carbon stocks
177 were quantified on an equivalent soil mass basis (Ellert and Bettany, 1995).



178

179 **Fig. 1.** Soil organic carbon content in both the agroforestry and agricultural control plot.
180 Associated errors are standard errors. N = 93 in the control, N = 40 in the agroforestry
181 tree row, N = 60 in the agroforestry alley. Data from Cardinael *et al.*, (2015b).

182

183 **2.2.2 Tree aboveground and stump carbon stocks**

184 Three hybrid walnuts were chopped down in 2012. The trunk circumference was measured
185 every meter up to the maximum height of the tree to estimate its volume. The trunk biomass
186 was estimated by multiplying the trunk volume by the wood density that was measured at 616
187 kg m⁻³ during a previous work at the same site (Talbot, 2011). Then, branches were cut, the
188 stump was uprooted, and they were weighted separately. Samples were brought to the
189 laboratory to determine the moisture content, which enabled calculation of the branches and the
190 stump dry mass.

191

192 **2.3 Measurements of organic carbon inputs in the field**

193 **2.3.1 Carbon inputs from tree fine root mortality**

194 The tree fine root (diameter ≤ 2 mm) biomass was quantified and coupled with an estimate of
195 the tree fine root turnover in order to predict the carbon input to the soil from the tree fine root
196 mortality. A detailed description of the methods used to estimate the tree fine root biomass can
197 be found in Cardinael *et al.*, (2015a). In March 2012, a 5 (length) \times 1.5 (width) \times 4 m (depth)
198 pit was open in the agroforestry plot, perpendicular to the tree row, at the North of the trees.
199 The tree fine root distribution was mapped down 4 m depth, and the tree fine root biomass was
200 quantified in the tree row and in the alley. Only results concerning the first two meters of soil,
201 among those obtained by Cardinael *et al.*, (2015a) will be used here.

202 In July 2012, sixteen minirhizotrons were installed in the agroforestry pit, at 0, 1, 2.5 and 4 m
203 depth, and at two and five meters from the trees. The tree root growth and mortality was

204 monitored during one year using a scanner (CI-600 Root Growth Monitoring System, CID,
205 USA), and analyzed using the WinRHIZO Tron software (Régent, Canada). A detailed
206 description of the methods and of results used to estimate the tree fine root turnover can be
207 found in Germon *et al.*, (2016).

208

209 **2.3.2 Tree litterfall**

210 In 2009, the crowns of two walnut trees were packed with a net in order to collect the leaf
211 biomass from September to January. The same was done in 2012 with three other walnut trees.
212 The leaf litter was then dried, weighted and analyzed for C to quantify the leaf carbon input per
213 tree.

214

215 **2.3.3 Aboveground and belowground input from the crop**

216 Since the tree planting in 1995, the crop yield was measured 14 times (in 1995, 2000, 2002,
217 2003, 2004, 2005, 2007, 2008, 2009, 2010, 2011, 2012, 2013, and 2014), while the wheat straw
218 biomass and the total aboveground biomass were measured six times (in 2007, 2008, 2009,
219 2011, 2012, and 2014) in both the control and the agroforestry plot (Dufour *et al.*, 2013), using
220 sampling subplots of 1 m² each. In the control plot, five subplots have been sampled while in
221 the agroforestry plot five transects have been sampled. Each transect was made of three
222 subplots, 2 m North from the tree, 2 m South from the tree, and 6.5 m from the tree (middle of
223 the alley). In March 2012, a 2 m deep pit was opened in the agricultural control plot (Prieto *et*
224 *al.*, 2015), and the root biomass was quantified to the maximum rooting depth (1.5 m). The
225 root:shoot ratio of durum wheat was measured in the control plot. We assumed that the crop
226 root biomass turns out once a year, after the crop harvest.

227

228 **2.3.4 Above and belowground input from the tree row herbaceous vegetation**

229 As two types of herbaceous vegetation grow in the tree rows during the year, samples were
 230 taken in summer and winter. In late June 2014, twelve subplots of 1 m² each were positioned
 231 in the tree rows, around 4 walnut trees. In January 2015, six subplots of 1 m² each were
 232 positioned in the tree rows, around 2 walnut trees. The middle of each subplot was located at 1
 233 m, 2 m and 3 m, respectively, from the selected walnut tree. All the aboveground vegetation
 234 was collected in each square. In the middle of each subplot, root biomass was sampled with a
 235 cylindrical soil corer (inner diameter of 8 cm). Soil was taken at three soil layers, 0.0-0.1, 0.1-
 236 0.3 and 0.3-0.5 m. In the laboratory, soil was gently washed with water through a 2 mm mesh
 237 sieve, and roots were collected. Roots from the herbaceous vegetation were easily separated
 238 manually from walnut roots, as they were soft and yellow compared to walnuts roots that were
 239 black. After being sorted out from the soil and cleaned, the root biomass was dried at 40°C and
 240 measured.

241

242 **2.4 Carbon concentration measurements**

243 All organic carbon measurements were performed with a CHN elemental analyzer (Carlo Erba
 244 NA 2000, Milan, Italy), after samples were oven-dried at 40°C for 48 hours (Table 2). Dry
 245 biomasses (t DM ha⁻¹) of each organic matter inputs were multiplied by their respective organic
 246 carbon concentrations (mg C g⁻¹) to calculate organic carbon stocks (t C ha⁻¹).

247

248 **Table 2.** Organic carbon concentrations and C:N ratio of the different types of biomass.

Type of biomass	Organic C concentration (mg C g ⁻¹)	C:N	Number of replicates
Walnut trunk	445.7 ± 1.0	159.1 ± 25.2	3
Walnut branches	428.6 ± 1.7	62.2 ± 11.7	3
Wheat straw	433.2 ± 0.7	55.5 ± 2.1	5
Wheat root	351.4 ± 19	24.8 ± 2.1	8
Walnut leaf	449.4 ± 3.7	49.1 ± 0.4	3
Walnut fine root	437.0 ± 3.3	28.6 ± 3.4	8
Summer vegetation (ABG)	448.4 ± 1.9	37.8 ± 2.2	5
Summer vegetation (roots)	314.5 ± 8.3	33.8 ± 1.7	6

Winter vegetation (ABG)	447.7 ± 5.3	11.2 ± 0.4	3
Winter vegetation (roots)	397.4 ± 5.0	24.7 ± 0.7	3

249 The organic matter called “vegetation” stands for the herbaceous vegetation that grows in the
 250 tree row. ABG: aboveground. Errors represent standard errors.

251

252 **2.5 General description of the CARBOSAF model**

253 **2.5.1 Organic carbon decomposition**

254 We adapted a model developed by Guenet et al. (2013) where total SOC is split in two pools,
 255 the FOC and the humified soil organic carbon (HSOC) for each soil layer (Fig. 1a). Input to the
 256 FOC pool comes from the plant litter and the distribution of this input within the profile is
 257 assumed to depend upon depth from the surface (z), distance from the tree (d), and time (t).
 258 Equations describing inputs to the FOC pool ($I_{t,z,d}$) at a given time, depth, and distance are
 259 fully explained in the Results.

260

261 The FOC mineralisation is assumed to be governed by first order kinetics, being proportional
 262 to the FOC pool, as given by:

$$263 \quad dec_FOC_{t,z,d} = -k_{FOC} \times FOC_{t,z,d} \times f_{clay,z} \times f_{moist,z} \times f_{temp,z} \quad (1)$$

264 where $FOC_{t,z,d}$ is the FOC carbon pool (kg C m^{-2}) at a given time (t , in years), depth (z , in m)
 265 and distance (d , in m), and k_{FOC} is its decomposition rate. The potential decomposition rates of
 266 the different plant materials were assessed with a 16-week incubation experiment during a
 267 companion study at the site (Prieto et al., 2016). The decomposition rate k_{FOC} was weighted by
 268 the respective contribution of each type of plant litter as a function of the tree age, soil depth
 269 and distance from the tree. The rate modifiers $f_{clay,z}$, $f_{moist,z}$ and $f_{temp,z}$ are functions depending
 270 respectively on the clay content, soil moisture and soil temperature at a given depth z , and range
 271 between 0 and 1.

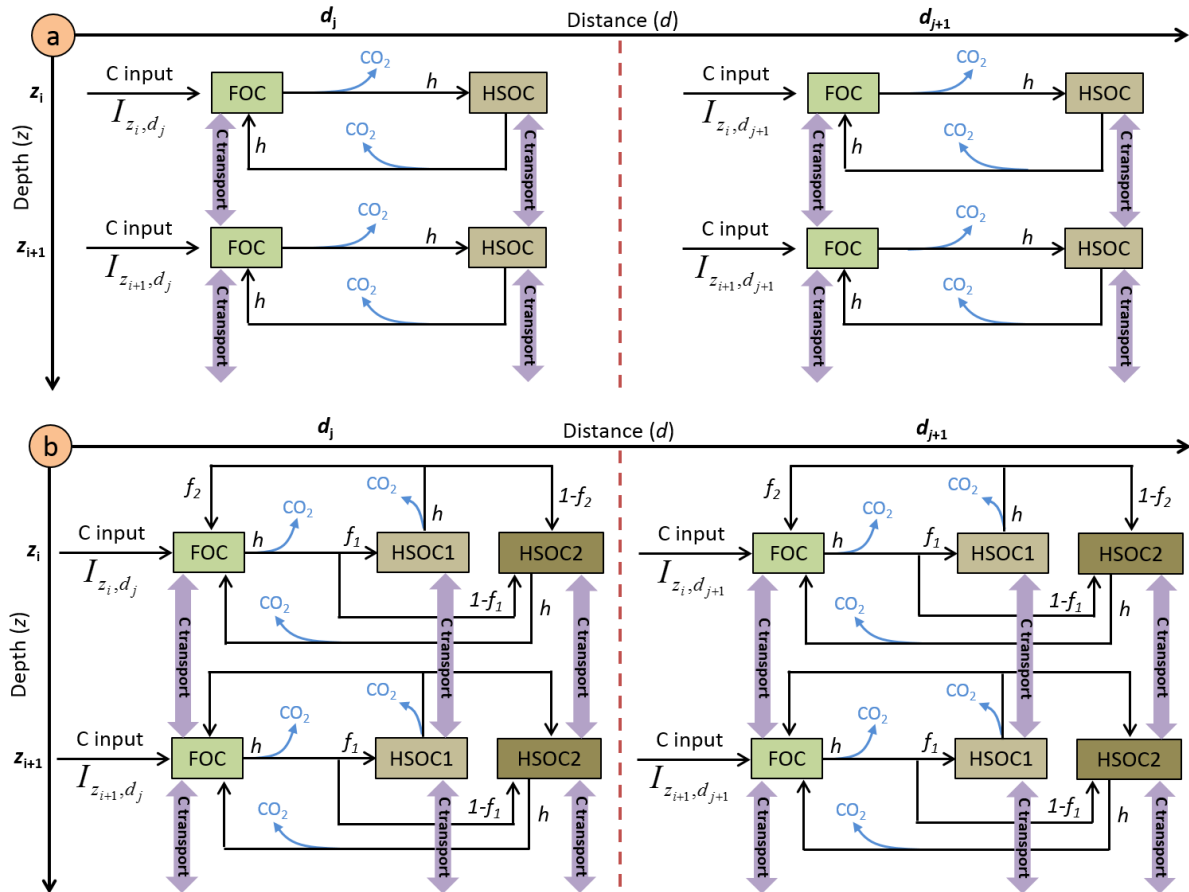
272

273 The f_{clay} function originated from the CENTURY model (Parton et al., 1987):

274
$$f_{clay,z} = 1 - 0.75 \times Clay_z \quad (2)$$

275 where $Clay_z$ is the clay fraction (ranging between 0 and 1) of the soil at a given depth z .

276



277

278 **Fig. 2.** Schematic representation of the pools and the fluxes of the (a) two pools model and (b)
 279 three pools model.

280

281 The $f_{moist,z}$ function originated from the meta-analysis of Moyano *et al.*, (2012) and is affected
 282 by soil properties (clay content, SOC content). Briefly, the authors fitted linear models on 310
 283 soil incubations to describe the effect of soil moisture on decomposition. Then, they normalized
 284 such linear models between 0 and 1 to apply these functions to classical first order kinetics. All
 285 details are described in Moyano *et al.*, (2012). To save computing time, we calculated $f_{moist,z}$

286 only once using measured SOC stocks instead of using modelled SOC stocks and repeated the
 287 calculation at each time step.

288

289 The temperature sensitivity of the soil respiration is expressed as Q_{10} :

$$290 \quad f_{temp,z} = Q_{10}^{\frac{temp_z - temp_{opt}}{10}} \quad (3)$$

291 with $temp_z$ being the soil temperature in K at each soil depth z and $temp_{opt}$ a parameter fixed to
 292 304.15 K. The Q_{10} value was fixed to 2, a classical value used in models (Davidson and
 293 Janssens, 2006).

294

295 Once the FOC is decomposed, a fraction is humified (h) and another is respired as CO₂ ($1-h$)
 296 (Fig. 2a) following equations (4) and (5).

$$297 \quad Humified\ FOC_{t,z,d} = h \times dec_FOC_{t,z,d} \quad (4)$$

$$298 \quad Respired\ FOC_{t,z,d} = (1 - h) \times dec_FOC_{t,z,d} \quad (5)$$

299

300 Two mathematical approaches are available in the model to describe the mineralisation of
 301 HSOC: a first order kinetics, as given by Eq. (6) or an approach developed by Wutzler &
 302 Reichstein, (2008) and by Guenet *et al.*, (2013) introducing the priming effect, i.e., the
 303 mineralisation of HSOC depends on FOC availability, and given by Eq. (7):

$$304 \quad dec_HSOC_{t,z,d} = -k_{HSOC,z} \times HSOC_{t,z,d} \times f_{moist,z} \times f_{temp,z} \quad (6)$$

$$305 \quad dec_HSOC_{t,z,d} = -k_{HSOC,z} \times HSOC_{t,z,d} \times (1 - e^{-PE \times FOC_{t,z,d}}) \times f_{moist,z}$$

$$306 \quad \times f_{temp,z} \quad (7)$$

307 where $HSOC_{t,z,d}$ is the humified SOC carbon pool at a given time (t , in years), depth (z , in m)
 308 and distance (d , in m), $k_{HSOC,z}$ is its decomposition rate (yr⁻¹) at a given depth z , and PE is the
 309 priming effect parameter. The parameters $f_{moist,z}$ and $f_{temp,z}$ are functions depending respectively
 310 on soil moisture and soil temperature at a given depth z , and affecting the decomposition rate

311 of HSOC. They correspond to the moisture equation from Moyano *et al.*, (2012) and to Eq. (3),
312 respectively. The decomposition rate $k_{HSOC,z}$ was an exponential law depending on soil depth
313 (z) as shown by an incubation study (see paragraph *HSOC decomposition rate* further in the
314 M&M):

$$315 \quad k_{HSOC,z} = a \times e^{-b \times z} \quad (8)$$

316 The b parameter of this equation represented the ratio of labile C/stable C within the HSOC
317 pool. The effect of clay on HSOC decomposition was implicitly taken into account in this
318 equation as clay content increased with soil depth.

319 A fraction of decomposed HSOC returns to the FOC assuming that part of the HSOC
320 decomposition products is as labile as FOC (h) and another is respired as CO₂ (Fig. 2a) in the
321 two pools model.

322

323 Finally, we also developed an alternative version of the model with three pools by splitting the
324 HSOC pools into two pools with different turnover rates, HSOC2 being more stabilized than
325 HSOC1 (Fig. 2b). The non-respired decomposed FOC is split between HSOC1 and HSOC2
326 following a parameter f_1 . The non-respired decomposed HSOC1 is split between HSOC2 and
327 FOC following a parameter f_2 whereas non-respired decomposed HSOC2 is only redistributed
328 into the FOC pools. The decomposition of HSOC1 and HSOC2 both follow the equation (8)
329 but with different parameter values for a .

330

331 **2.5.2 Carbon transport mechanisms**

332 The transport of C between the different soil layers was represented by both advection and
333 diffusion mechanisms (Elzein and Balesdent, 1995), which have been shown to usually describe
334 well the C transport in soils (Bruun *et al.*, 2007; Guenet *et al.*, 2013). The advection represents
335 the C transport due to the water infiltration in the soil, while the diffusion represents the C

336 transport due to the fauna activity. The same transport coefficients were applied to the two C
337 pools, FOC and HSOC.

338

339 The advection is defined by:

$$340 \quad F_A = A \times C \quad (9)$$

341 where F_A is the flux of C transported downwards by advection, and A is the advection rate (mm
342 yr^{-1}).

343

344 The diffusion is represented by the Fick's law:

$$345 \quad F_D = -D \times \frac{\partial^2 C}{\partial z^2} \quad (10)$$

346 where F_D is the flux of C transported downwards by diffusion, $-D$ the diffusion coefficient (cm^2
347 yr^{-1}) and C the amount of carbon in the pool subject to transport (FOC or HSOC).

348

349 To represent the effect of soil tillage ($z \leq 0.2$ m), we added another diffusion term using the
350 Fick's law but with a value of D several orders of magnitude higher to represent the mixing due
351 to tillage. It must be noted that no tillage effect on the decomposition was represented here
352 because of the large unknowns on these aspects (Dimassi et al., 2013; Virto et al., 2012).

353

354 In this model, the flux of C transported downwards by the advection and diffusion (F_{AD}) was
355 represented as the sum of both mechanisms, following Elzein & Balesdent (1995):

$$356 \quad F_{AD} = F_A + F_D \quad (11)$$

357

358 The FOC and HSOC pools dynamics in the two pools model correspond to:

$$359 \quad \frac{\partial FOC_{t,z,d}}{\partial t} = I_{t,z,d} + \frac{\partial F_{AD}}{\partial z} + h \times dec_HSOC_{t,z,d} - dec_FOC_{t,z,d} \quad (12)$$

$$360 \quad \frac{\partial HSOC_{t,z,d}}{\partial t} = \frac{\partial F_{AD}}{\partial z} + h \times dec_FOC_{t,z,d} - dec_HSOC_{t,z,d} \quad (13)$$

361

362 Finally, the FOC, HSOC1 and HSOC2 pools dynamics in the three pools model correspond to:

$$363 \quad \frac{\partial FOC_{t,z,d}}{\partial t} = I_{t,z,d} + \frac{\partial F_{AD}}{\partial z} + h \times f_2 \times dec_HSOC1_{t,z,d} + h \times dec_HSOC2_{t,z,d}$$

$$364 \quad - dec_FOC_{t,z,d} \quad (14)$$

$$365 \quad \frac{\partial HSOC1}{\partial t} = \frac{\partial F_{AD}}{\partial z} + h \times f_1 \times dec_FOC_{t,z,d} - dec_HSOC1_{t,z,d} \quad (15)$$

$$366 \quad \frac{\partial HSOC2}{\partial t} = \frac{\partial F_{AD}}{\partial z} + h \times (1 - f_1) \times dec_FOC_{t,z,d} + h \times (1 - f_2) \times dec_HSOC1_{t,z,d}$$

$$367 \quad - dec_HSOC2_{t,z,d} \quad (16)$$

368

369 2.5.3 Depth dependence of HSOC potential decomposition rates

370 The shape of the function (i.e. the b parameter) describing the HSOC potential decomposition
 371 rate (Eq. (8)) was determined by incubating soils from the control, the alley and the tree row,
 372 and from different soil layers (0.0-0.1, 0.1-0.3, 0.7-1.0 and 1.6-1.8 m). Soils were sieved at 5
 373 mm, and incubated during 44 days at 20°C at a water potential of -0.03 MPa. Evolved CO₂ was
 374 measured using a micro-GC at 1, 3, 7, 14, 21, 28, 35, 44 days. The three first measurement
 375 dates corresponded to a pre-incubation period and were not included in the analysis. For a given
 376 depth, the cumulative mineralised SOC was expressed as a percentage of total SOC and was
 377 plotted against the incubation time. The slopes represented the potential SOC mineralisation
 378 rate at a given soil depth and location. The potential SOC mineralisation rates were then plotted
 379 against soil depth (Fig. S1). We used the soil incubations to determine only the b parameter of
 380 the curve: with such short term incubations, the SOC decomposition rate over the soil profile
 381 is overestimated because the CO₂ measured during the incubations mainly originates from the
 382 labile C pool. The a parameter was optimized following the procedure described further.

383

384 **2.6 Boundary conditions of the CARBOSAF model**

385 **2.6.1 Annual aggregates of soil temperature and soil moisture**

386 In April 2013, eight soil temperature and moisture sensors (Campbell CS 616 and Campbell
387 107, respectively) were installed in the agroforestry plot at 0.3, 1.3, 2.8 and 4.0 m depth, and at
388 2 and 5 m from the trees. Soil temperature and moisture were measured for 11 months.

389 The mean annual soil temperature in the agroforestry plot was described by the following
390 equation:

$$391 \quad T = -0.89 \times z + 288.24 \quad (R^2 = 0.99) \quad (17)$$

392 where T is the soil temperature (K) and z is the soil depth (m).

393

394 The mean annual soil moisture was described with the following equation:

$$395 \quad \theta = 0.05 \times z + 0.28 \quad (R^2 = 0.99) \quad (18)$$

396 where θ is the soil volumetric moisture (cm cm^{-3}) and z is the soil depth (m).

397 Due to a lack of data in the agricultural plot, we assumed that the soil temperature and the soil
398 moisture were the same in the agroforestry tree rows, alleys and in the control plot, but we
399 further performed a sensitivity analysis of the model on these two parameters.

400

401 **2.6.2 Interpolation of tree growth**

402 The tree growth has been measured in the field since the establishment of the experiment. We
403 used the diameter at breast height (DBH) as a surrogate of the tree growth preferentially to the
404 tree height as the field measurements were more accurate. Indeed, DBH is easier to measure
405 than height, especially when trees are getting older. To describe the temporal dynamic of DBH
406 since the tree planting, a linear equation was fitted on the data.

407 Tree growth measurements enabled us to fit the following equation that was used in the model:

408
$$DBH_t \begin{cases} 0.01, & t \leq 3 \\ 0.0157 \times t - 0.0391 & (R^2 = 0.997) \quad 3 < t \leq 20 \end{cases} \quad (19)$$

409 where DBH_t is the diameter at breast height (m) and t represents the time since tree planting
410 (years).

411

412 **2.6.3 Change of tree litterfall over time**

413 For the five walnut trees where the leaf biomass was quantified, DBH was also measured. The
414 ratio between the leaf biomass and DBH was then calculated for the five replicates. Total leaf
415 biomass was 8.96 ± 1.45 kg DM tree⁻¹ and the carbon concentration of walnut leaves was 449.4
416 ± 3.7 mg C g⁻¹ (Table 2). With a density of 110 trees ha⁻¹, leaf litterfall was estimated at $0.73 \pm$
417 0.06 t C ha⁻¹ in 2012 and at the plot scale. The ratio between leaf biomass and DBH was 0.0277
418 ± 0.0024 t C tree⁻¹ m⁻¹ or 3.05 t C ha⁻¹ m⁻¹. The following linear relationship was therefore used
419 in the model to describe leaf litter C input with the tree growth:

420
$$L_t = 3.05 \times DBH_t \quad (20)$$

421 where L_t is the leaf litter input (t C ha⁻¹) at the year t , and DBH_t the diameter at breast height
422 (m) the year t .

423

424 **2.6.4 Tree fine root C input from mortality**

425 In 2012, the measured tree fine root biomass was higher in the tree row than in the alley (Table
426 S1). From 0 to 1 m distance from the tree (in the tree row), the tree fine root biomass was
427 homogeneous and was 1.01 t C ha⁻¹ down 2 m depth.

428 In 2012 and in the alley, the tree fine root biomass ($TFRB$) decreased with increasing distance
429 from the tree and was represented by an exponential function:

430
$$TFRB = \begin{cases} 1.01, & 0 \leq d \leq 1 \\ 1.29 \times e^{-0.28 \times d} & (R^2 = 0.90), \quad 1 < d \leq 6.5 \end{cases} \quad (21)$$

431 where $TFRB$ represents tree fine root biomass down 2 m depth (t C ha⁻¹), and d the distance
 432 from the tree (m).

433

434 We considered a linear increase of $TFRB$ with increasing DBH , and a linear regression was
 435 performed between $TFRB$ in 2012 and $TFRB$ in 1996, the first year after planting (biomass
 436 considered as negligible). The following linear relationship was used to simulate $TFRB$ as a
 437 function of tree growth:

$$438 \quad TFRB_{t,d} = \begin{cases} 3.69 \times DBH_t, & 0 \leq d \leq 1 \\ 4.70 \times DBH_t \times e^{-0.28 \times d}, & 1 < d \leq 6.5 \end{cases} \quad (22)$$

439 where $TFRB_t$ represents the tree fine root biomass to 2 m depth (t C ha⁻¹) at the year t , DBH_t the
 440 diameter at breast height (m) at the year t , and d the distance to the tree (m).

441

442 A changing distribution of tree fine roots within the soil profile was taken into account with
 443 increasing distance to the tree. For this purpose, exponential functions ($a \times e^{-b \times z}$) were
 444 fitted in the alley every 0.5 m distance, and a linear regression was fitted between their
 445 coefficients a and b and distance from the tree. However, the distribution of $TFRB$ within the
 446 soil profile and with the distance to the tree was considered constant with time.

447 A decreasing exponential function best represented the changing distribution of tree fine roots
 448 within the soil profile with increasing distance to the tree:

$$449 \quad p_{TFRB,z,d} = \begin{cases} 13.92 \times e^{-1.39 \times z} & (R^2 = 0.68), & 0 \leq d \leq 1 \\ a \times e^{-b \times z}, & & 1 < d \leq 6.5 \end{cases} \quad (23)$$

450 and

$$451 \quad a = 10.31 - 1.15 \times d \quad (R^2 = 0.69) \quad (24)$$

$$452 \quad b = -1.10 + 0.19 \times d \quad (R^2 = 0.51) \quad (25)$$

453 Finally,

$$454 \quad p_{TFRB,z,d} = \begin{cases} 13.92 \times e^{-1.39 \times z}, & 0 \leq d \leq 1 \\ (10.31 - 1.15 \times d) \times e^{-(-1.10 + 0.19 \times d) \times z}, & 1 < d \leq 6.5 \end{cases} \quad (26)$$

455 where $p_{TFRB,z,d}$ is the proportion (%) of the total tree fine root biomass ($TFRB$) at a given depth
456 z (m), and at a distance d from the tree (m).

457

458 To finally estimate the tree fine root input due to the mortality, $TFRB$ was multiplied by the
459 measured root turnover. The tree fine root turnover ranged from 1.7 to 2.8 yr^{-1} depending on
460 fine root diameter, with an average turnover of 2.2 yr^{-1} for fine roots ≤ 2 mm and to a depth of
461 2 m (Germon et al., 2016).

462

463 **2.6.5 Aboveground and belowground input from the crop**

464 As there were more crop yield measurements (14) than straw biomass measurements (6), the
465 effect of agroforestry on the crop yield with time was used as an estimate for change in the
466 aboveground and belowground wheat biomass.

467 For this, the relative yield ($Rel Y_{AF}$) in the agroforestry system was calculated for each year as
468 the ratio between the agroforestry yield and the control yield (Y_C).

469 The average annual crop yield in the control plot was $Y_C = 3.79 \pm 0.40$ t DM ha^{-1} for the 14
470 studied years. In the agroforestry plot, the average relative yield decreased linearly with time
471 (increasing DBH) and was described using the following linear equation (Fig. 3):

$$472 \quad Rel Y_{AF_t} = -93.33 \times DBH_t + 100 \quad (R^2 = 0.12, \quad p - value = 0.02) \quad (27)$$

473 where $Rel Y_{AF_t}$ is the average relative crop yield (%) in the agroforestry plot compared to the
474 control plot at year t , and DBH_t is the diameter at breast height (m) at year t .

475

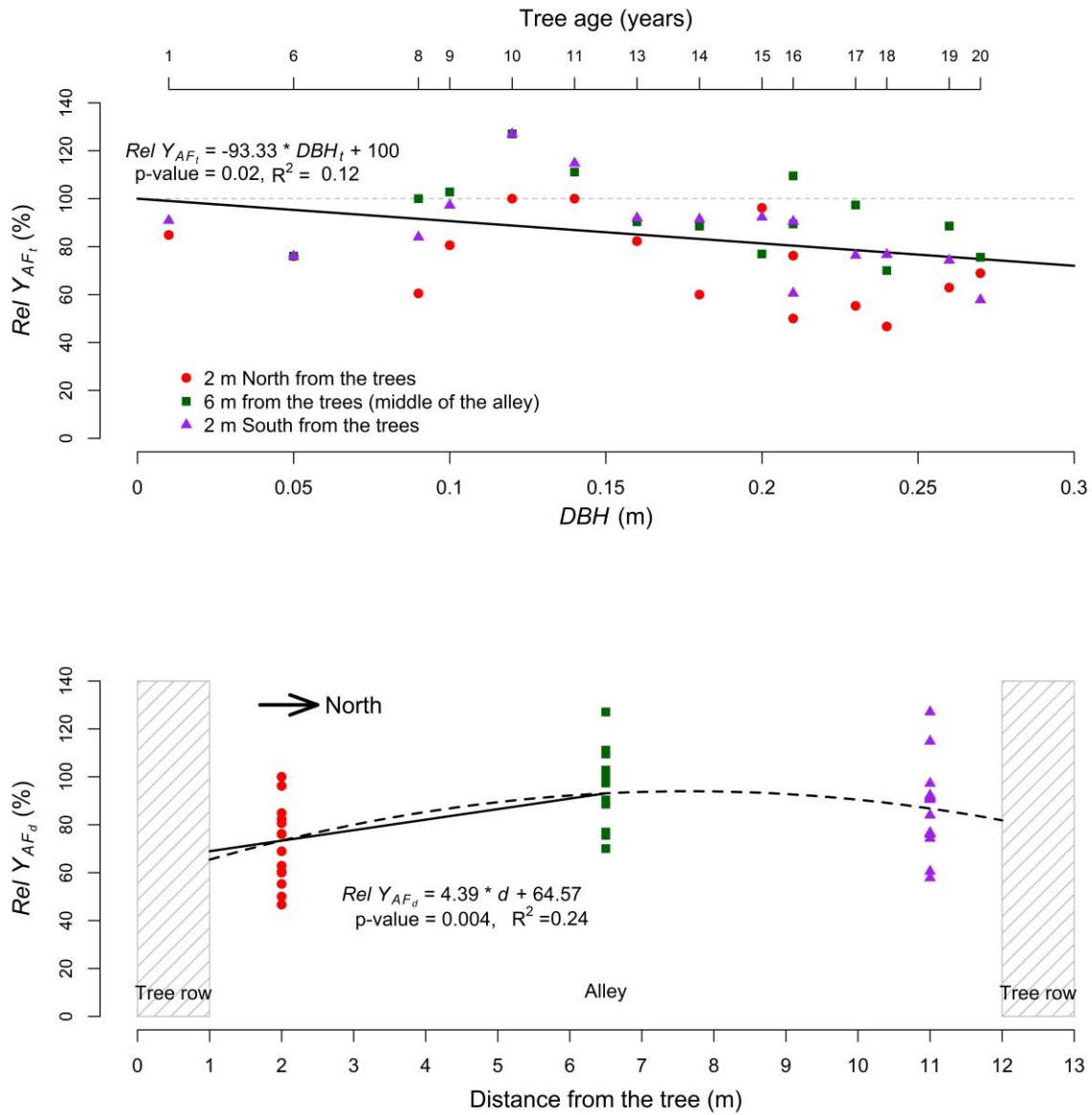
476 The variation of crop yield with distance from the trees was described with a quadratic equation
477 (Fig. 2). But as we aimed to predict SOC stocks up to 6.5 m distance from the trees (middle of
478 the alley), a linear increase of crop yield with increasing distance from the tree gave similar

479 results as the quadratic equation over the 6.5 m distance and was more parsimonious:

480 $Rel Y_{AF_d} = 4.39 \times d + 64.57 \quad (R^2 = 0.24), \quad 1 < d \leq 6.5 \quad (28)$

481 where $Rel Y_{AF_d}$ is the relative crop yield (%) in the agroforestry plot at a distance d (m) from

482 the tree compared to the control plot.



483
484 **Fig. 3.** Top: Relative yield ($Rel Y_{AF_t}$) in the agroforestry plot compared to the control plot as a

485 function of tree growth, represented by the diameter at breast height (DBH) at year t . Bottom:

486 Relative yield ($Y_{AF_{t,d}}$) as a function of the distance from the tree.

487

488 Finally, the crop yield in the agroforestry plot was modeled as follows:

$$489 \quad Y_{AF,t,d} = Rel Y_{AF_t} \times Y_C \times Rel Y_{AF_d} \quad (R^2 = 0.19), \quad 1 < d \leq 6.5 \quad (29)$$

490 where $Y_{AF,t,d}$ is the crop yield (t DM ha⁻¹) in the agroforestry plot at the year t and at a distance
491 d (m) from the tree. Because three linear equations were used to describe the crop yield in the
492 agroforestry plot, errors were accumulated and we finally came up with a standard
493 underestimation of the crop yield in the agroforestry plot that we corrected by multiplying our
494 equation by 1.2.

495

496 The ratio between the straw biomass and the crop yield was calculated as the average of the six
497 measurements, and was considered constant with time. This ratio was used to convert crop yield
498 into straw biomass. In the agroforestry plot, the carbon input to the soil from the aboveground
499 crop biomass was:

$$500 \quad ABC_{crop,t,d} = Y_{AF,t,d} \times (straw\ biomass: crop\ yield) \times C_{straw} \times (1 - export) \quad (30)$$

501 where $ABC_{crop,t,d}$ is the aboveground carbon input from the crop (t C ha⁻¹) at the year t and
502 distance d from the tree, $Y_{AF,t,d}$ is the agroforestry crop yield. The average ratio between the
503 straw biomass (t DM ha⁻¹) and the crop yield (t DM ha⁻¹) equaled 1.03 ± 0.11 (n=6). The wheat
504 straw was exported out of the field after the harvest, but it was estimated that 25% of the straw
505 biomass was left on the soil, thus $export=0.75$. In the control plot, $Y_{AF,t,d}$ was replaced by Y_C .

506 To estimate fine root biomass of the crop, we hypothesized that the root:shoot ratio of the durum
507 wheat was the same in both the agroforestry and agricultural plot, in the absence of any
508 published data on the matter. In the agroforestry plot, the belowground crop biomass was
509 represented by:

$$510 \quad BEC_{crop,t,d} = Y_{AF,t,d} \times (shoot: crop\ yield) \times (root: shoot) \times C_{root} \quad (31)$$

511 where $BEC_{crop,t,d}$ is the belowground crop biomass (t C ha⁻¹) at the year t and at a distance d
512 from the tree, $Y_{AF,t,d}$ is the agroforestry crop yield. The average ratio between the total crop

513 aboveground biomass (*shoot*) and the crop yield equaled 2.45 ± 0.15 (n=6). In 2012, total fine
 514 root biomass was 2.29 ± 0.32 t C ha⁻¹ in the control (Table 3).

515

516 **Table 3.** Wheat fine root biomass in the agricultural control plot in 2012.

Soil depth (m)	Wheat fine root biomass	
	(kg C m ⁻³)	(t C ha ⁻¹)
0.0-0.1	0.48 ± 0.05	0.48 ± 0.05
0.1-0.3	0.34 ± 0.04	0.69 ± 0.09
0.3-0.5	0.22 ± 0.04	0.44 ± 0.08
0.5-1.0	0.10 ± 0.04	0.52 ± 0.20
1.0-1.5	0.03 ± 0.04	0.17 ± 0.19
Total	-	2.29 ± 0.32

517 Errors represent standard errors.

518

519 Therefore, the wheat *root:shoot* ratio equaled 0.79 ± 0.12 (n=1). The carbon concentration of
 520 wheat root was $C_{root} = 35.14 \pm 1.90$ mg C g⁻¹. In the control plot, $Y_{AF,t,d}$ was replaced by Y_C .

521

522 In 2012, no wheat roots were observed below 1.5 m, and root biomass decreased exponentially
 523 with increasing depth (Table 3). The distribution of crop roots within the soil profile was
 524 described as follows:

$$525 \quad p_{CRBc,z} = \begin{cases} 26.44 \times e^{-2.59 \times z} & (R^2 = 0.99), & z \leq 1.5 \\ 0, & & z > 1.5 \end{cases} \quad (32)$$

526 where $p_{CRBc,z}$ is the proportion (%) of total crop root biomass in the control plot at a given
 527 depth z (m).

528 Since the same maximum rooting depth of the crop was observed in the agroforestry plot and
 529 in the control plot, we inferred that the wheat root distribution within the soil profile was not
 530 modified by agroforestry, but only its biomass. The crop root turnover was assumed to be 1 yr⁻¹,
 531 root mortality occurring mainly after crop harvest.

532

533

534 2.6.6 Aboveground and belowground input from herbaceous vegetation in the tree rows

535 The distance from the trees had no effect on the above and belowground biomass of the
536 herbaceous vegetation (data not shown), therefore average values are presented. The summer
537 aboveground biomass was almost three times higher than in winter, whereas the belowground
538 biomass was two times higher (Table 4). The total aboveground carbon input was 2.13 ± 0.14 t
539 $\text{C ha}^{-1} \text{ yr}^{-1}$ and the total belowground carbon input was 0.74 ± 0.05 t $\text{C ha}^{-1} \text{ yr}^{-1}$ to 0.5 m depth.

540

541 **Table 4.** Aboveground and belowground biomass of the herbaceous vegetation in the tree rows.

	Soil depth (m)	Herbaceous biomass (t C ha ⁻¹)	
		Summer	Winter
Aboveground	-	1.57 ± 0.11	0.56 ± 0.09
Belowground	0.0-0.1	0.22 ± 0.03	0.17 ± 0.01
	0.1-0.3	0.16 ± 0.02	0.06 ± 0.01
	0.3-0.5	0.09 ± 0.04	0.04 ± 0.01
	Total	0.46 ± 0.04	0.27 ± 0.02

542 Errors represent standard errors.

543

544 The belowground carbon input from the tree row vegetation ($BEC_{veg,z}$, t C ha⁻¹) at a given depth
545 z (m) was described by the following equation:

$$546 \quad BEC_{veg,z} = \begin{cases} 0.44 \times e^{-3.12 \times z}, & z \leq 1.5 \\ 0, & z > 1.5 \end{cases} \quad (33)$$

547 We assumed for simplification that the aboveground and belowground biomasses of the
548 herbaceous vegetation in the tree row were constant over time.

549

550 2.7 Optimization procedure

551 Depending on the model variant, four to five parameters were optimized with a gradient based
552 statistical method (Santaren et al., 2007; Tarantola, 1987, 2005) using measured SOC stocks
553 from the control plot only. These parameters were A , the advection rate, D , the diffusion

554 coefficient, h the humification yield, a the coefficient of the k_{HSOC} rate from Eq. (10), and PE
555 the priming coefficient. These four or five parameters were calibrated so that equilibrium SOC
556 stocks, i.e. after 5000 years of simulation, equaled SOC stocks of the control plot in 2013. The
557 associated uncertainty was estimated with the 93 soil cores sampled in the control plot (see
558 section 2.2.1). Due to a lack of relevant data, we assumed that the climate and the land use were
559 the same for the last 5000 years, and that SOC stocks in the control plot were at equilibrium at
560 the time of measurement. Therefore, SOC stocks at the end of the 5000 years of simulation
561 equaled SOC stocks in the control plot. Three different calibrations were performed,
562 corresponding to the three model variants that were used: one calibration with the two pools
563 model without the priming effect, one calibration with the two pools model with the priming
564 effect, and one calibration with the three pools model.

565 Each model variant was fitted to the control SOC stocks data using a curve fitting method
566 described in Tarantola (1987), after a conversion from SOC stocks in kg C m^{-2} to SOC stocks
567 in kg m^{-3} due to the different soil layers' thickness. We aimed to find a parameter set that
568 minimizes the distance between model outputs and the corresponding observations, considering
569 model and data uncertainties, and starting parameter information. With the assumption of
570 Gaussian errors for both the observations and the starting parameters, the optimal parameter set
571 corresponds to the minimum of the cost function $J(\mathbf{x})$:

$$572 \quad J(\mathbf{x}) = 0.5 \times [(\mathbf{y} - \mathbf{H}(\mathbf{x}))^t \times \mathbf{R}^{-1} \times (\mathbf{y} - \mathbf{H}(\mathbf{x})) + (\mathbf{x} - \mathbf{x}_b)^t \times \mathbf{P}_b^{-1} \times (\mathbf{x} - \mathbf{x}_b)] \quad (34)$$

573 that contains both the mismatch between modelled and observed SOC stock and the mismatch
574 between a starting and optimized parameters. \mathbf{x} is the vector of unknown parameters, \mathbf{x}_b the
575 vector of a starting parameter values fixed for each optimization procedures, $\mathbf{H}()$ the model and
576 \mathbf{y} the vector of observations. The covariance matrices \mathbf{P}_b and \mathbf{R} describe a priori uncertainties
577 on parameters, and observations, respectively. Both matrices are diagonal as we suppose the
578 observation uncertainties and the parameter uncertainties to be independent. The covariance

579 matrices \mathbf{P}_b are presented in Table S2. To determine an optimal set of parameters which
580 minimizes $\mathbf{J}(\mathbf{x})$, we used the BFGS gradient-based algorithm (Tarantola, 1987). For each model
581 variant, we performed 30 optimizations starting with different starting parameter values to
582 check that the results did not correspond to a local minimum. As the BFGS algorithm does not
583 directly calculate the variance of posteriors, they were quantified using the curvature cost
584 function at its minimum once it was reached (Santaren et al., 2007).

585

586 2.8 Comparison of models

587 Model predictions with and without priming effect were compared calculating the coefficients
588 of determination, root mean square errors (RMSE) and Bayesian information criteria (BIC).

$$589 \quad RMSE = \sqrt{\frac{1}{N} \sum_{i=1}^N (x_i - \bar{x})^2} \quad (35)$$

590 where i is the number of observations (1 to N), x_i is the predicted value and \bar{x} is the mean
591 observed value.

$$592 \quad BIC = k \times \ln(N) - 2 \times \ln(\hat{L}) \quad (36)$$

593 where N is the number of observations, k is the number of model parameters, and \hat{L} is the
594 maximized value of the likelihood function of the model (Schwarz, 1978).

595

596 The model was run at a yearly time step using mean annual soil temperature and moisture and
597 annual C inputs to the soil. In the agroforestry, the model was run from the ground (0 m) to 2
598 m depth, and from the tree (0 m) to 6.5 m from the tree (middle of the alley). The model was
599 applied separately across locations of a tree-distance gradient having varying OC inputs, each
600 soil column was considered independent from another. SOC pools were initialized after a spin-
601 up of 5000 years in the control plot. At t_0 , SOC stocks in the agroforestry plot therefore equaled

602 SOC stocks of the control plot. The model was then run from t_0 to t_{18} (years) after tree planting.
603 The spatial resolution was 0.1 m both vertically and horizontally. The model was developed
604 using R 3.1.1 (R Development Core Team, 2013). Partial-differential equations were solved
605 using the R package *deSolve* and the *ode.ID* method (Soetaert et al., 2010).

606

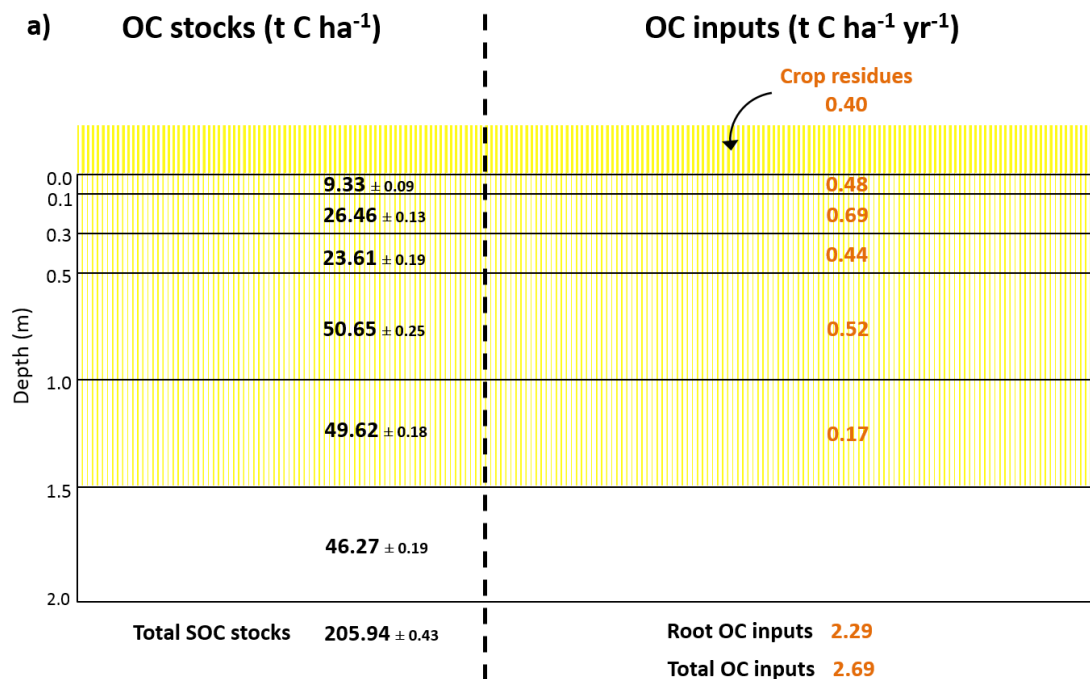
607 **3 Results**

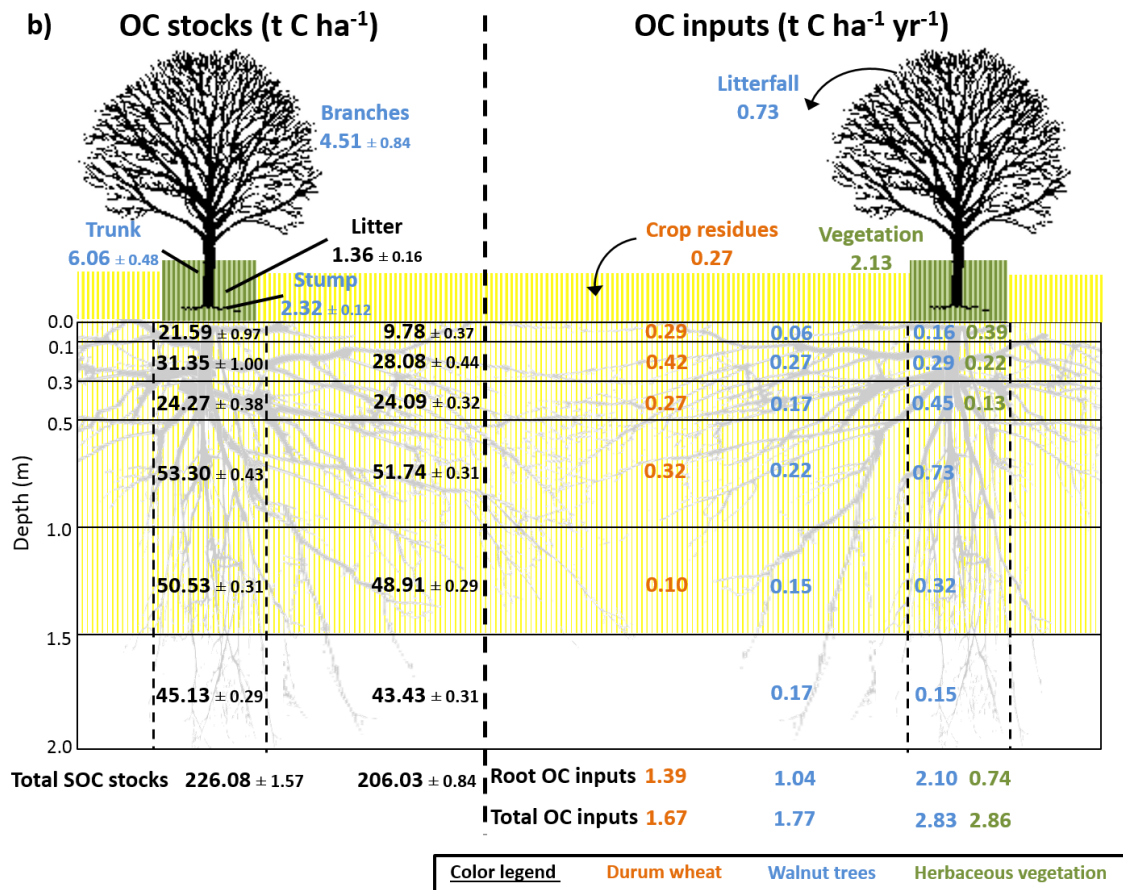
608 **3.1 Organic carbon inputs and SOC stocks: a synthesis from field measurements**

609 In the alleys of the 18-year-old agroforestry system, measured organic carbon (OC) inputs from
610 the crop residues and roots were reduced compared to the control plot due a lower crop yield
611 (Fig. 4). This reduction in crop OC inputs was offset by OC inputs from the tree roots and tree
612 litterfall. Total root OC inputs in the alleys (crop + tree roots) and in the control plot (crop roots)
613 were very similar, respectively 2.43 and 2.29 t C ha⁻¹ yr⁻¹. Alleys received 0.60 t C ha⁻¹ yr⁻¹
614 more of total aboveground biomass (crop residues + tree litterfall) than the control, which was
615 added to the plough layer. Tree rows received 2.35 t C ha⁻¹ yr⁻¹ more C inputs in the first 0.3 m
616 of soil compared to the control plot, mainly from the herbaceous vegetation. Down the whole
617 soil profile, tree rows received two times more OC inputs compared to the control plot (Fig. 4),
618 and 65% more than alleys. Overall, the agroforestry plot had 41% more OC inputs to the soil
619 than the control plot to 2 m depth (3.80 t C ha⁻¹ yr⁻¹ compared to 2.69 t C ha⁻¹ yr⁻¹). In the
620 agroforestry plot, the largest aboveground OC input to the soil comes from the herbaceous
621 vegetation, and not from the trees. In the control plot, 85% of OC inputs are wheat root litters.
622 In the agroforestry plot, root inputs represent 71% of OC inputs in the alleys, and 50% in the
623 tree rows.

624 In the first 0.3 m of soil, SOC stocks were significantly higher in the alleys than in the control
625 plot, but the difference was small (2.1 ± 0.6 t C ha⁻¹). Between 0.3 and 1.0 m, the difference of
626 SOC stocks was smaller but still significant. However, between 1 and 2 m depth, SOC stocks

627 were significantly lower in the alleys than in the control. As a consequence, there was no
 628 significant difference of total SOC stocks between the two locations down the whole soil
 629 profile. In the tree rows, topsoil organic carbon stocks (0.0-0.3 m) were much higher than in
 630 the control ($+ 17.0 \pm 1.4 \text{ t C ha}^{-1}$). This positive difference of SOC stocks decreased with depth
 631 but remained significantly positive down 1.5 m depth. The opposite was observed between 1.5
 632 and 2.0 m depth. Delta of total SOC stocks between the tree rows and the control plot was 20.1
 633 $\pm 1.6 \text{ t C ha}^{-1}$. At the plot scale, total SOC stocks were significantly higher in the agroforestry
 634 plot compared to the control plot down 2 m depth ($+ 3.3 \pm 0.9 \text{ t C ha}^{-1}$).





637

638 **Fig. 4.** Measured soil organic carbon stocks and organic carbon inputs to the soil a) in the

639 agricultural control plot, b) in the 18-year-old agroforestry plot. Associated errors are

640 standard errors. Values are expressed per hectare of land type (control, alley, tree row).

641 To get the values per hectare of agroforestry, data from alley and tree row have to be

642 weighted by their respective surface area (i.e., 84% and 16%, respectively) and then

643 added up. OC: organic carbon; SOC: soil organic carbon. SOC stocks data are issued

644 from Cardinael *et al.*, (2015a), data of tree root OC inputs are combined from Cardinael

645 *et al.*, (2015b) and from Germon *et al.*, (2016).

646

647 3.2 HSOC decomposition rate

648 The soil incubation experiment showed that the HSOC mineralization rate decreased

649 exponentially with depth (Fig. S1) and could be described with:

650
$$k_{HSOC,z} = 6.114 \times e^{-1.37 \times z} \quad (R^2 = 0.76) \quad (37)$$

651 where z is the soil depth (m), and where the a (yr^{-1}) coefficient ($a = 6.114$) was further optimized

652 (Table 5).

653

654 **Table 5.** Summary of optimized model parameters.

Model parameter	Meaning	Starting parameter range	Posterior values \pm variance (starting parameter values)		
			2 pools - without <i>PE</i>	2 pools - with <i>PE</i>	3 pools – without <i>PE</i>
<i>a</i>	coefficient from Eq. (8) of the HSOC decomposition (yr^{-1})	3.65e-6-3.65	$0.01\text{e}^{-2} \pm <10^{-4}$ (0.01e ⁻²)	$0.01\text{e}^{-2} \pm <10^{-4}$ (0.01e ⁻²)	-
<i>a</i> ₁	coefficient from Eq. (8) of the HSOC1 decomposition (yr^{-1})	3.65e-6-3.65	-	-	$0.01\text{e}^{-2} \pm <10^{-4}$ (0.01e ⁻²)
<i>a</i> ₂	coefficient from Eq. (8) of the HSOC2 decomposition (yr^{-1})	3.65e-6-3.65	-	-	$0.83\text{e}^{-2} \pm 0.17\text{e}^{-2}$ (0.83e ⁻²)
<i>D</i>	diffusion coefficient ($\text{cm}^2 \text{yr}^{-1}$)	1e-6-1	$4.62\text{e}^{-4} \pm 5.95\text{e}^{-4}$ (9.64e ⁻⁴)	$5.63\text{e}^{-4} \pm 1.42\text{e}^{-4}$ (9.01e ⁻⁴)	$5.24\text{e}^{-4} \pm 7.62\text{e}^{-4}$ (9.64e ⁻⁴)
<i>A</i>	advection rate (mm yr^{-1})	1e-6-1	$21.25\text{e}^{-4} \pm 5.02\text{e}^{-4}$ (8.54e ⁻⁴)	$6.63\text{e}^{-4} \pm 2.38\text{e}^{-4}$ (4.27e ⁻⁴)	$21.60\text{e}^{-4} \pm 2.24\text{e}^{-4}$ (8.54e ⁻⁴)
<i>h</i>	humification yield	0.01-1	$0.32 \pm <10^{-4}$ (0.34)	$0.25 \pm 1.00\text{e}^{-4}$ (0.13)	0.34 ± 0.03 (0.34)
<i>PE</i>	priming coefficient	0.1-160	-	9.66 ± 1.49 (102.95)	-
<i>f</i> ₁	fraction of decomposed FOC entering the HSOC1 pool	0-1	-	-	0.99 ± 0.18 (0.86)
<i>f</i> ₂	fraction of decomposed HSOC1 entering the FOC pool	0-1	-	-	$0.94 \pm 1.10\text{e}^{-3}$ (0.80)

655 The starting parameter range represents the range in which starting parameter values were sampled for the 30 optimizations per model variant. The
656 starting parameter values presented in brackets in the posterior column represent the starting parameter values that minimized the $\mathbf{J}(\mathbf{x})$ value (Eq.
657 (34)).

659 3.3 Modeling results

660 3.3.1 Optimized parameters and correlation matrix

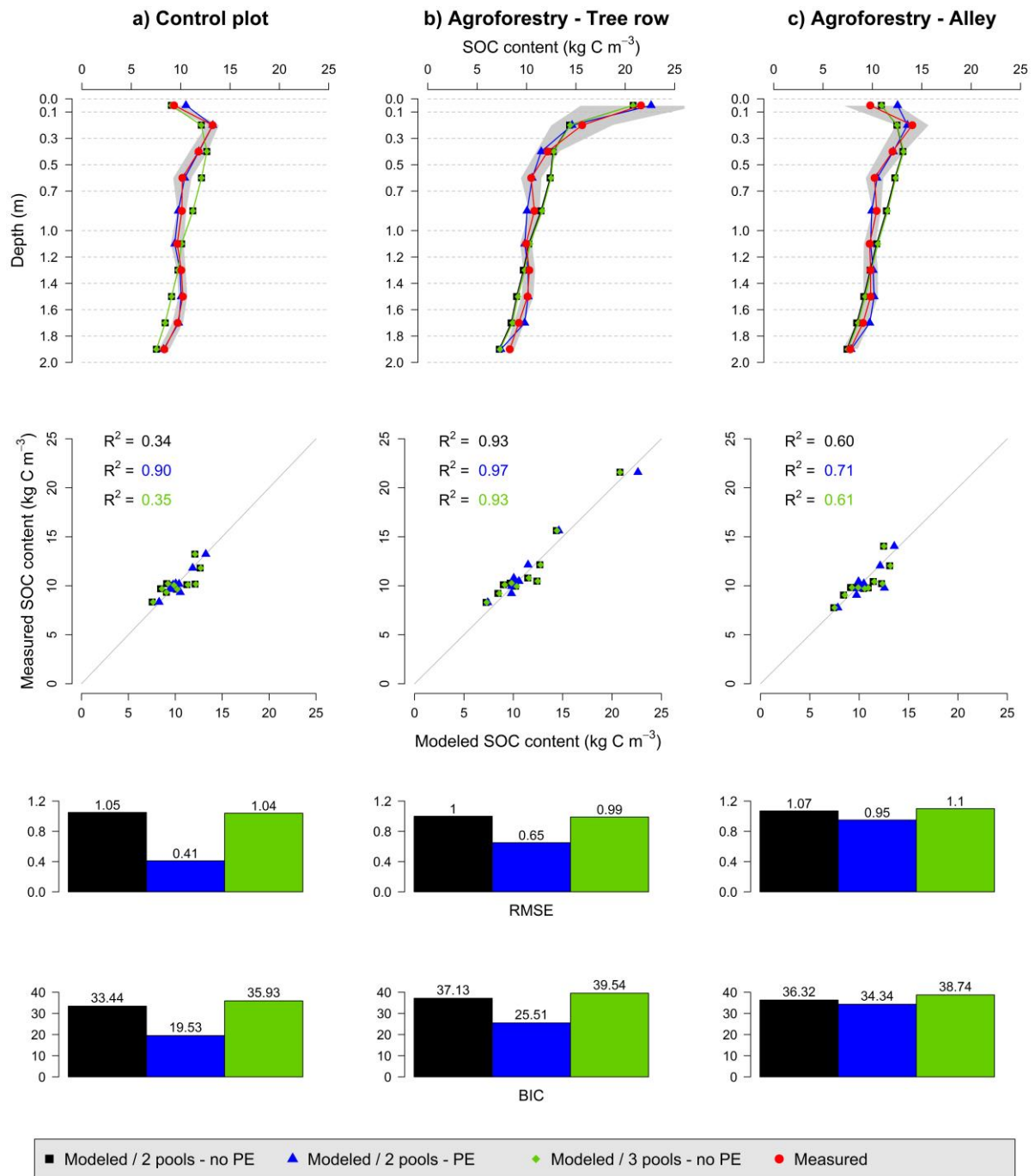
661 The optimized parameters and their starting parameter modes are presented in [Table 5](#). For the
662 two pools model without priming effect, the most important correlation was observed between
663 h and A which control the humification and the transport by advection. Concerning the two
664 pools model with priming effect, the most important correlations were observed between h and
665 PE which controls the effect of the FOC on HSOC decomposition, and between h and A . A and
666 PE were also positively correlated ([Fig. S2](#)). For the three pools model, f_1 and f_2 were by
667 definition negatively correlated, but f_2 and A were also correlated. Considering the method used
668 to optimize the parameters, these important correlation factors hinder the presentation of the
669 model output within an envelope. Therefore, we presented the model results using the optimized
670 parameter without any envelope.

671

672 3.3.2 Modeled SOC stocks

673 As a reminder, SOC stocks of the agroforestry plot were not part of model calibration (that used
674 the control plot only) but were used here for validation. Observed SOC stocks were not well
675 represented by the two pools model without priming effect, with RMSE ranging from 1.00 to
676 1.07 kg C m^{-3} ([Fig. 5, Table S3](#)). The model performed better when the priming effect was
677 taken into account, with RMSE ranging from 0.41 to 0.95 kg C m^{-3} , and the SOC profile was
678 well described. The representation of SOC stocks was not improved by the inclusion of a third
679 C pool in the model. Overall, the two pools model with priming effect was the best one, as
680 shown by the BICs ([Fig. 5, Table S3](#)). For all models, SOC stocks below 1 m depth were better
681 described than above SOC stocks ([Table S3](#)). The spatial distribution of SOC stocks and of
682 additional SOC storage was also well described ([Fig. 6](#)), with a very high additional SOC
683 storage in the topsoil layer in the tree row. Most modeled SOC storage in the agroforestry plot

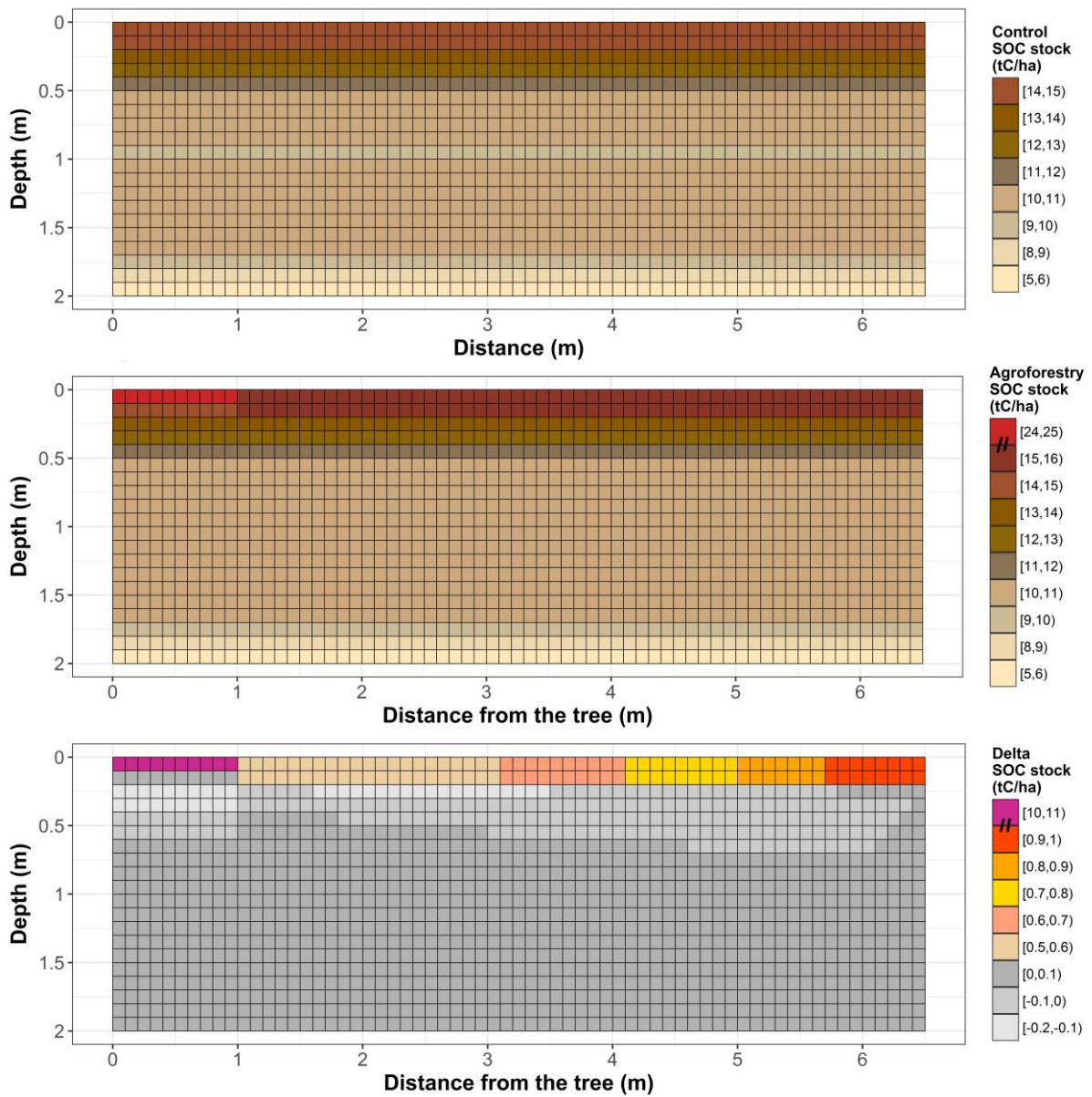
684 was located in the first 0.2 m depth, but SOC storage was slightly higher in the middle of the
 685 alleys than in the alleys close to the tree rows.



686

687 **Fig. 5.** Measured and modeled soil organic carbon contents (kg C m⁻³) in an agricultural control
 688 plot and in an 18-year-old silvoarable system with a two pools model without priming effect
 689 (no *PE*), with a two pools model with priming effect (*PE*) and with a three pools model without

690 PE. Gray shaded bands represent standard deviations of measured SOC stocks (n=93 in the
 691 control, n=40 in the tree rows, and n=60 in the alleys).



692
 693 **Fig. 6.** Spatial distribution of control SOC stocks (top), agroforestry SOC stocks (middle), and
 694 additional SOC storage ($t\ C\ ha^{-1}$) in an 18-year-old silvoarable system compared to an
 695 agricultural control plot and represented by the two pools model with priming effect. The
 696 scale used in the middle and bottom panels are not continuous due to the
 697 large stocks predicted by the model in the top layer in the tree-row.

698

699 **4 Discussion**

700 **4.1 OC inputs drive SOC storage in agroforestry systems**

701 Increased SOC stocks in the agroforestry plot compared to the control may be explained either
702 by increased OC inputs, or decreased OC outputs by SOC mineralization, or both. In the alleys,
703 higher SOC stocks in the topsoil could be explained by inputs from litterfall and tree roots
704 despite a decrease in crop inputs. Most of additional SOC storage in the agroforestry plot was
705 found in the topsoil in the tree rows. The same distribution was observed for OC inputs to the
706 soil. Inputs from the herbaceous vegetation had an important impact on SOC storage. The
707 increased SOC stocks in the tree rows were largely explained by an important above-ground
708 carbon input ($2.13 \text{ t C ha}^{-1} \text{ yr}^{-1}$) by the herbaceous vegetation between trees. This result had
709 already been suggested by Cardinael et al., (2015b) and by Cardinael et al., (2017) who showed
710 that even young agroforestry systems could store SOC in the tree rows while trees are still very
711 small. These “grass strips” indirectly introduced by the tree planting in parallel tree rows have
712 a major impact on SOC stocks of agroforestry systems. Increased SOC stocks below the plough
713 layer could be explained by higher root inputs, but these inputs could also have contributed to
714 decrease SOC stocks below 1.5 m due to priming effect. At the plot scale, measured organic
715 carbon inputs to the soil were increased by 40% ($+1.1 \text{ t C ha}^{-1} \text{ yr}^{-1}$) down 2 m depth in the 18-
716 year-old agroforestry plot compared to the control plot, resulting in increased SOC stocks of
717 3.3 t C ha^{-1} . Increased OC inputs in agroforestry systems has been shown in other studies but
718 they were only quantified in the first 20 cm of soil (Oelbermann et al., 2006; Peichl et al., 2006).
719 This study is therefore the first one also quantifying deep OC inputs to soil. In this study and
720 due to a lack of data, soil temperature and soil moisture were considered the same in both plots
721 so that abiotic factors controlling SOC decomposition were identical. Reduced soil temperature
722 is often observed in agroforestry systems (Clinch et al., 2009; Dubbert et al., 2014), but effect

723 of agroforestry on soil moisture is much more complex. The soil evaporation is reduced under
724 the trees, but soil water is also lost through the transpiration of trees (Ilstedt et al., 2016; Ong
725 and Leakey, 1999). These opposing effects vary with the distance from the tree (Odhiambo et
726 al., 2001). Moreover, increased water infiltration and water storage has been observed under
727 the trees after a rainy event (Anderson et al., 2009). Therefore, the effect of agroforestry on soil
728 moisture is variable in time and space, and should be investigated more in details. Interactions
729 between soil temperature and soil moisture on the SOC decomposition are known to be complex
730 (Conant et al., 2011; Moyano et al., 2013; Sierra et al., 2015). A sensitivity analysis performed
731 on these two boundary conditions showed that the model was not very sensitive to soil
732 temperature and soil moisture (Fig. S3), but the real effect of these two parameters on SOC
733 dynamics under agroforestry systems should be specifically investigated in future studies.
734 Despite these simplifying assumptions on similarities in microclimate but also on vertical
735 transport between the control and the agroforestry system, the model calibrated to the control
736 plot was able to reproduce SOC stocks in tree rows and alleys and its depth distribution well.
737 This strong validation also revealed that OC inputs were sufficient to explain the differences in
738 SOC stocks at this site. Furthermore, the SOC decomposition rate could also be modified due
739 to an absence of soil tillage in the tree rows (Balesdent et al., 1990) or to an increased aggregate
740 stability (Udawatta et al., 2008) in the topsoil.

741

742 **4.2 Representation of SOC spatial heterogeneity in agroforestry systems**

743 The lateral spatial heterogeneity of SOC stocks in the agroforestry plot was well described by
744 the two pools model including priming effect, with higher SOC stocks in the tree rows' topsoil
745 than in the alleys. The model treated the carbon from the tree row herbaceous litter as an input
746 to the upper layer of the mineral soil, in the same way as inputs by roots. Introduction of
747 nitrogen in the model could be further tested in order to take into account a lower carbon use

748 efficiency due to a lack of nutrients for microbial growth in this litter. The strong SOC gradient
749 observed in the topsoil in tree rows compared to the used resolution could lead to numerical
750 errors. We therefore tested a finer grid resolution, and results were very similar, suggesting
751 some robustness of the model. For all models, SOC stocks were better described in the tree
752 rows than in the alleys. In the alleys, the spatial distribution of organic inputs is more complex
753 and thus more difficult to model. The tree root system is influenced by the soil tillage and by
754 the competition with the crop roots, and thus the highest tree fine root density is not observed
755 in the topsoil but in the 0.3-0.5 m soil layer (Cardinael et al., 2015a). In the model, we were not
756 able to represent this specific tree root pattern with commonly used mathematical functions,
757 and tree root profiles were modeled, by default, using a decreasing exponential. Indeed,
758 piecewise linear functions introduce threshold effects not desirable for transport mechanisms,
759 especially diffusion. This simplification could partly explain the model overestimation of SOC
760 stocks in the 0.0-0.1 m layer of the alleys compared to observed data. This result suggests that
761 it could be useful to couple the CARBOSAF model with a model describing root architecture
762 and root growth (Dunbabin et al., 2013; Dupuy et al., 2010), using for instance voxel automata
763 (Mulia et al., 2010). Moreover, the model described a slight increase of SOC stocks in the
764 middle of the alleys than close to the trees in the alleys. This could be explained by the linear
765 equation used to describe the crop yield as a function of the distance from the trees, leading to
766 an overestimation of the crop yield reduction close to the trees. It could also be explained by
767 the formalism used to model leaf litter distribution in the plot. We considered a homogeneous
768 distribution of leaf inputs in the agroforestry plot, which was the case in the last years, but
769 probably not in the first years of the tree growth where leaves might be more concentrated close
770 to the trees (Thevathasan and Gordon, 1997).

771 The two pools model with priming effect also represented a slight SOC storage in the
772 agroforestry plot below 1.0 m depth, but it was not observed in the field. This could be linked

773 to an overestimation of C input from tree fine root mortality. Indeed, a constant root turnover
774 was considered along the soil profile, but several authors reported a decrease of the root
775 turnover with increasing soil depth (Germon et al., 2016; Hendrick and Pregitzer, 1996; Joslin
776 et al., 2006). However, the sensitivity analysis showed that the model was not sensitive to this
777 parameter (Fig. S3).

778

779 **4.3 Vertical representation of SOC profiles in models**

780 The best model to represent SOC profiles considered the priming effect. This process can act
781 in two different ways on the shape of SOC profiles. It has a direct effect on the SOC
782 mineralization and it therefore modulates the amount of SOC in each soil layer, creating
783 different SOC gradients. This indirectly affects the mechanisms of C transport within the soil
784 profile, as shown by a modification of transport coefficients in the case of priming effect (Table
785 5). Contrary to what was shown by Cardinael *et al.*, (2015c) in long term bare fallows receiving
786 contrasted organic amendments, the addition of another SOC pool could not surpass the
787 inclusion of priming effect in terms of model performance. Together with Wutzler &
788 Reichstein, (2013) and Guenet *et al.*, (2016), this study therefore suggests that implementing
789 priming effect into SOC models would improve model performances especially when
790 modelling deep SOC profiles.

791 We considered here the same transport coefficients for the FOC and HSOC pools, but the
792 quality and the size of OC particles are different, potentially leading to various movements in
793 the soil by water fluxes or fauna activity (Lavelle, 1997). Moreover, we considered identical
794 transport parameters in the agroforestry and in the control plot, but the presence of trees could
795 modify soil structure, soil water fluxes (Anderson et al., 2009), and the fauna activity (Price
796 and Gordon, 1999). However, the model was little sensitive to these parameters (Fig. S3).

797 Further study could investigate the role of different transport coefficients on the description of
798 SOC profiles.

799

800 **4.4 Higher OC inputs or a different quality of OC?**

801 The introduction of trees in an agricultural field not only modifies the amount of litter residues,
802 but also their quality. Tree leaves, tree roots, and the herbaceous vegetation from the tree row
803 have different C:N ratios, lignin and cellulose contents than the crop residues. Recent studies
804 showed that plant diversity had a positive impact on SOC storage (Lange et al., 2015; Steinbeiss
805 et al., 2008). One of the hypothesis proposed by the authors is that diverse plant communities
806 result in more active, more abundant and more diverse microbial communities, increasing
807 microbial products that can potentially be stabilized. In our model, litter quality is not related
808 to different SOC pools, but is implicitly taken into account in the FOC decomposition rate,
809 which is weighted by the respective contribution from the different types of OC inputs. To test
810 this, we performed a model run considering that all OC inputs in the agroforestry plot were crop
811 inputs (all FOC decomposition rates equaled wheat decomposition rate), but results were not
812 significantly different from the one presented here. Hence, we considered that changes in litter
813 quality in the agroforestry plot did not significantly influence SOC decomposition rates.

814

815 **4.5 Possible limitation of SOC storage by priming effect**

816 Our modelling results suggested that the priming effect could considerably reduce the capacity
817 of soils to store organic carbon. Our study showed that the increase of SOC stocks was not
818 proportional to OC inputs, especially at depth. This result has often been observed in Free Air
819 CO₂ Enrichment (FACE) experiments. In these experiments, productivity is usually increased
820 due to CO₂ fertilization, but several authors also reported an increase in SOC decomposition
821 but not linearly linked to the productivity increase (van Groenigen et al., 2014; Sulman et al.,

822 2014). In a long-term FACE experiment, Carney *et al.*, (2007) also found that SOC decreased
823 due to priming effect, offsetting 52% of additional carbon accumulated in aboveground and
824 coarse root biomass. The priming effect intensity also relies on nutrient availability (Zhang *et*
825 *al.*, 2013). In agroforestry systems, tree roots can intercept leached nitrate below the crop
826 rooting zone (Andrianarisoa *et al.*, 2016), reducing nutrient availability. This beneficial
827 ecosystem service could indirectly increase the priming effect intensity in deep soil layers.
828 The formalism used here to simulate priming effect assumes that there is no mineralisation of
829 the SOC in the absence of fresh OC inputs (no basal respiration). This is a strong hypothesis,
830 but this situation never occurs since the FOC pool is never empty (data not shown). In the alleys
831 and below the maximum rooting depth of crops, there are no direct inputs of FOC, but OC is
832 transported in these deep layers due to transport mechanisms. However, further studies could
833 study the impact of the priming effect formalism on the estimation of its intensity by using
834 explicit microbial biomass for instance (Blagodatsky *et al.*, 2010; Perveen *et al.*, 2014).
835 Finally, root exudates were not quantified in this study. Several authors showed that they could
836 induce strong priming effects (Bengtson *et al.*, 2012; Keiluweit *et al.*, 2015), but root exudates
837 are also a source of labile carbon, potentially contributing to stable SOC (Cotrufo *et al.*, 2013).
838 These opposing effects of root exudates on SOC should be further investigated, especially
839 concerning the deep roots in agroforestry systems.

840

841 **5 Conclusions**

842 We proposed the first model that simulates soil organic carbon dynamics in agroforestry
843 accounting for both the whole soil profile and the lateral spatial heterogeneity in agroforestry
844 plots. The two pools model with priming effect described reasonably well the measured SOC
845 stocks after 18 years of agroforestry and SOC distributions with depth. It showed that the
846 increased inputs of fresh biomass to soil in the agroforestry system explained the observed

847 additional SOC storage and suggested priming effect as a process controlling SOC stocks in the
848 presence of trees. This study points out at processes that may be modified by deep rooting trees
849 and deserve further studies given their potential effects on SOC dynamics, such as additional
850 inputs of C as roots exudates, or altered soil structure leading to modified SOC transport rates.

851

852 **6 Data availability**

853 The data and the model are freely available upon request and can be obtained by contacting the
854 author (remi.cardinael@cirad.fr).

855

856 **Information about the Supplement**

857 The Supplement includes the walnut tree fine root biomass (Table S1), the covariance matrices
858 P_b of optimized parameters (Table S2), the different model performances (Table S3), the
859 potential SOC decomposition rate as a function of soil depth (Fig. S1), the correlation matrices
860 of optimized parameters (Fig. S2), and a sensitivity analysis of the model (Fig. S3).

861

862 *Acknowledgments.*

863 This study was financed by the French Environment and Energy Management Agency
864 (ADEME), following a call for proposals as part of the REACCTIF program (Research on
865 Climate Change Mitigation in Agriculture and Forestry). This work was part of the funded
866 project AGRIPSOL (Agroforestry for Soil Protection, 1260C0042), coordinated by Agrooif.
867 Rémi Cardinael was supported both by ADEME and by La Fondation de France. We thank the
868 farmer, Mr Breton, who allowed us to sample in his field. We are very grateful to our colleagues
869 for their work in the field since the tree planting, especially Jean-François Bourdoncle, Myriam
870 Dauzat, Lydie Dufour, Jonathan Mineau, Alain Sellier and Benoit Suard. We thank colleagues
871 and students who helped us for measurements in the field or in the laboratory, especially Daniel

872 Billiou, Cyril Girardin, Patricia Mahafaka, Agnès Martin, Valérie Pouteau, Alexandre Rosa,
873 and Manon Villeneuve. Finally, we would like to thank Jérôme Balesdent, Pierre Barré and
874 Philippe Peylin for their valuable comments on the modeling part of this work.

875

876 **References**

877 Ahrens, B., Braakhekke, M. C., Guggenberger, G., Schrumpf, M. and Reichstein, M.:
878 Contribution of sorption, DOC transport and microbial interactions to the ^{14}C age of a soil
879 organic carbon profile: Insights from a calibrated process model, *Soil Biol. Biochem.*, 88, 390–
880 402.

881 Albrecht, A. and Kandji, S. T.: Carbon sequestration in tropical agroforestry systems, *Agric.*
882 *Ecosyst. Environ.*, 99, 15–27, 2003.

883 Anderson, S. H., Udawatta, R. P., Seobi, T. and Garrett, H. E.: Soil water content and infiltration
884 in agroforestry buffer strips, *Agrofor. Syst.*, 75(1), 5–16, 2009.

885 Andrianarisoa, K., Dufour, L., Bienaime, S., Zeller, B. and Dupraz, C.: The introduction of
886 hybrid walnut trees (*Juglans nigra* x *regia* cv. NG23) into cropland reduces soil mineral N
887 content in autumn in southern France, *Agrofor. Syst.*, 90(2), 193–205, 2016.

888 Baisden, W. T. and Parfitt, R. L.: Bomb ^{14}C enrichment indicates decadal C pool in deep soil?,
889 *Biogeochemistry*, 85, 59–68, 2007.

890 Baisden, W. T., Amundson, R., Brenner, D. L., Cook, A. C., Kendall, C. and Harden, J. W.: A
891 multiisotope C and N modeling analysis of soil organic matter turnover and transport as a
892 function of soil depth in a California annual grassland soil chronosequence, *Global*
893 *Biogeochem. Cycles*, 16(4), 82-1-82–26, 2002.

894 Balandier, P. and Dupraz, C.: Growth of widely spaced trees. A case study from young
895 agroforestry plantations in France, *Agrofor. Syst.*, 43, 151–167, 1999.

896 Balesdent, J., Mariotti, A. and Boissgonnier, D.: Effect of tillage on soil organic carbon
897 mineralization estimated from ^{13}C abundance in maize fields, *J. Soil Sci.*, 41(4), 587–596, 1990.

898 Bambrick, A. D., Whalen, J. K., Bradley, R. L., Cogliastro, A., Gordon, A. M., Olivier, A. and
899 Thevathasan, N. V: Spatial heterogeneity of soil organic carbon in tree-based intercropping
900 systems in Quebec and Ontario, Canada, *Agrofor. Syst.*, 79, 343–353, 2010.

901 Bengtson, P., Barker, J. and Grayston, S. J.: Evidence of a strong coupling between root
902 exudation, C and N availability, and stimulated SOM decomposition caused by rhizosphere
903 priming effects, *Ecol. Evol.*, 2(8), 1843–1852, 2012.

904 Blagodatsky, S., Blagodatskaya, E., Yuyukina, T. and Kuzyakov, Y.: Model of apparent and
905 real priming effects: Linking microbial activity with soil organic matter decomposition, *Soil*
906 *Biol. Biochem.*, 42(8), 1275–1283, 2010.

907 Braakhekke, M. C., Beer, C., Hoosbeek, M. R., Reichstein, M., Kruijt, B., Schrumppf, M. and
908 Kabat, P.: SOMPROF: A vertically explicit soil organic matter model, *Ecol. Modell.*, 222(10),
909 1712–1730, 2011.

910 Bruun, S., Christensen, B. T., Thomsen, I. K., Jensen, E. S. and Jensen, L. S.: Modeling vertical
911 movement of organic matter in a soil incubated for 41 years with ^{14}C labeled straw, *Soil Biol.*
912 *Biochem.*, 39(1), 368–371, 2007.

913 Burgess, P. J., Incoll, L. D., Corry, D. T., Beaton, A. and Hart, B. J.: Poplar (*Populus* spp)
914 growth and crop yields in a silvoarable experiment at three lowland sites in England, *Agrofor.*
915 *Syst.*, 63, 157–169, 2004.

916 Cardinael, R., Mao, Z., Prieto, I., Stokes, A., Dupraz, C., Kim, J. H. and Jourdan, C.:
917 Competition with winter crops induces deeper rooting of walnut trees in a Mediterranean alley
918 cropping agroforestry system, *Plant Soil*, 391, 219–235, 2015a.

919 Cardinael, R., Chevallier, T., Barthès, B. G., Saby, N. P. A., Parent, T., Dupraz, C., Bernoux,

920 M. and Chenu, C.: Impact of alley cropping agroforestry on stocks, forms and spatial
921 distribution of soil organic carbon - A case study in a Mediterranean context, *Geoderma*, 259–
922 260, 288–299, 2015b.

923 Cardinael, R., Eglin, T., Guenet, B., Neill, C., Houot, S. and Chenu, C.: Is priming effect a
924 significant process for long-term SOC dynamics? Analysis of a 52-years old experiment,
925 *Biogeochemistry*, 123, 203–219, 2015c.

926 Cardinael, R., Chevallier, T., Cambou, A., Béral, C., Barthès, B. G., Dupraz, C., Durand, C.,
927 Kouakoua, E. and Chenu, C.: Increased soil organic carbon stocks under agroforestry: A survey
928 of six different sites in France, *Agric. Ecosyst. Environ.*, 236, 243–255, 2017.

929 Carney, K. M., Hungate, B. A., Drake, B. G. and Megonigal, J. P.: Altered soil microbial
930 community at elevated CO₂ leads to loss of soil carbon, *PNAS*, 104(12), 4990–4995, 2007.

931 Charbonnier, F., le Maire, G., Dreyer, E., Casanoves, F., Christina, M., Dauzat, J., Eitel, J. U.
932 H., Vaast, P., Vierling, L. A. and Roupsard, O.: Competition for light in heterogeneous
933 canopies: Application of MAESTRA to a coffee (*Coffea arabica* L.) agroforestry system,
934 *Agric. For. Meteorol.*, 181, 152–169, 2013.

935 Chaudhry, A. K., Khan, G. S., Siddiqui, M. T., Akhtar, M. and Aslam, Z.: Effect of arable crops
936 on the growth of poplar (*Populus deltoides*) tree in agroforestry system, *Pakistan J. Agric. Sci.*,
937 40, 82–85, 2003.

938 Chiffot, V., Bertoni, G., Cabanettes, A. and Gavaland, A.: Beneficial effects of intercropping
939 on the growth and nitrogen status of young wild cherry and hybrid walnut trees, *Agrofor. Syst.*,
940 66(1), 13–21, 2006.

941 Clinch, R. L., Thevathasan, N. V., Gordon, A. M., Volk, T. A. and Sidders, D.: Biophysical
942 interactions in a short rotation willow intercropping system in southern Ontario, Canada, *Agric.*
943 *Ecosyst. Environ.*, 131(1–2), 61–69, 2009.

944 Conant, R. T., Ryan, M. G., Ågren, G. I., Birge, H. E., Davidson, E. A., Eliasson, P. E., Evans,
945 S. E., Frey, S. D., Giardina, C. P., Hopkins, F. M., Hyvönen, R., Kirschbaum, M. U. F.,
946 Lavallee, J. M., Leifeld, J., Parton, W. J., Megan Steinweg, J., Wallenstein, M. D., Martin
947 Wetterstedt, J. Å. and Bradford, M. A.: Temperature and soil organic matter decomposition
948 rates - synthesis of current knowledge and a way forward, *Glob. Chang. Biol.*, 17(11), 3392–
949 3404, 2011.

950 Cotrufo, M. F., Wallenstein, M. D., Boot, C. M., Deneff, K. and Paul, E.: The Microbial
951 Efficiency-Matrix Stabilization (MEMS) framework integrates plant litter decomposition with
952 soil organic matter stabilization: do labile plant inputs form stable soil organic matter?, *Glob.*
953 *Chang. Biol.*, 19(4), 988–95, 2013.

954 Davidson, E. A. and Janssens, I. A.: Temperature sensitivity of soil carbon decomposition and
955 feedbacks to climate change, *Nature*, 440, 165–173, 2006.

956 Dimassi, B., Cohan, J.-P., Labreuche, J. and Mary, B.: Changes in soil carbon and nitrogen
957 following tillage conversion in a long-term experiment in Northern France, *Agric. Ecosyst.*
958 *Environ.*, 169, 12–20, 2013.

959 Dubbert, M., Mosena, A., Piayda, A., Cuntz, M., Correia, A. C., Pereira, J. S. and Werner, C.:
960 Influence of tree cover on herbaceous layer development and carbon and water fluxes in a
961 Portuguese cork-oak woodland, *Acta Oecologica*, 59, 35–45, 2014.

962 Dufour, L., Metay, A., Talbot, G. and Dupraz, C.: Assessing Light Competition for Cereal
963 Production in Temperate Agroforestry Systems using Experimentation and Crop Modelling, *J.*
964 *Agron. Crop Sci.*, 199(3), 217–227, 2013.

965 Dunbabin, V. M., Postma, J. A., Schnepf, A., Pagès, L., Javaux, M., Wu, L., Leitner, D., Chen,
966 Y. L., Rengel, Z. and Diggle, A. J.: Modelling root-soil interactions using three-dimensional
967 models of root growth, architecture and function, *Plant Soil*, 372(1–2), 93–124, 2013.

968 Dupuy, L., Gregory, P. J. and Bengough, A. G.: Root growth models: Towards a new generation
969 of continuous approaches, *J. Exp. Bot.*, 61(8), 2131–2143, 2010.

970 Duursma, R. and Medlyn, B.: MAESPA: a model to study interactions between water
971 limitation, environmental drivers and vegetation function at tree and stand levels, with an
972 example application to [CO₂] × drought interactions, *Geosci. Model Dev.*, 5, 919–940, 2012.

973 Eilers, K. G., Debenport, S., Anderson, S. and Fierer, N.: Digging deeper to find unique
974 microbial communities: The strong effect of depth on the structure of bacterial and archaeal
975 communities in soil, *Soil Biol. Biochem.*, 50, 58–65, 2012.

976 Eissenstat, D. M. and Yanai, R. D.: The Ecology of Root Lifespan, *Adv. Ecol. Res.*, 27, 1–60,
977 1997.

978 Ellert, B. H. and Bettany, J. R.: Calculation of organic matter and nutrients stored in soils under
979 contrasting management regimes, *Can. J. Soil Sci.*, 75, 529–538, 1995.

980 Elzein, A. and Balesdent, J.: Mechanistic simulation of vertical distribution of carbon
981 concentrations and residence times in soils, *Soil Sci. Soc. Am. J.*, 59, 1328–1335, 1995.

982 Fierer, N., Schimel, J. P. and Holden, P. A.: Variations in microbial community composition
983 through two soil depth profiles, *Soil Biol. Biochem.*, 35(1), 167–176, 2003.

984 Fontaine, S., Barot, S., Barré, P., Bdioui, N., Mary, B. and Rumpel, C.: Stability of organic
985 carbon in deep soil layers controlled by fresh carbon supply, *Nature*, 450, 277–281, 2007.

986 Germon, A., Cardinael, R., Prieto, I., Mao, Z., Kim, J. H., Stokes, A., Dupraz, C., Laclau, J.-P.
987 and Jourdan, C.: Unexpected phenology and lifespan of shallow and deep fine roots of walnut
988 trees grown in a silvoarable Mediterranean agroforestry system, *Plant Soil*, 401, 409–426, 2016.

989 Graves, A. R., Burgess, P. J., Palma, J. H. N., Herzog, F., Moreno, G., Bertomeu, M., Dupraz,
990 C., Liagre, F., Keesman, K., van der Werf, W., de Nooy, a. K. and van den Briel, J. P.:
991 Development and application of bio-economic modelling to compare silvoarable, arable, and

992 forestry systems in three European countries, *Ecol. Eng.*, 29(4), 434–449, 2007.

993 Graves, A. R., Burgess, P. J., Palma, J., Keesman, K. J., van der Werf, W., Dupraz, C., van
994 Keulen, H., Herzog, F. and Mayus, M.: Implementation and calibration of the parameter-sparse
995 Yield-SAFE model to predict production and land equivalent ratio in mixed tree and crop
996 systems under two contrasting production situations in Europe, *Ecol. Modell.*, 221, 1744–1756,
997 2010.

998 van Groenigen, K. J., Qi, X., Osenberg, C. W., Luo, Y. and Hungate, B. A.: Faster
999 decomposition under increased atmospheric CO₂ limits soil carbon storage, *Science.*, 344, 508–
1000 509, 2014.

1001 Guenet, B., Eglin, T., Vasilyeva, N., Peylin, P., Ciais, P. and Chenu, C.: The relative importance
1002 of decomposition and transport mechanisms in accounting for soil organic carbon profiles,
1003 *Biogeosciences*, 10(4), 2379–2392, 2013.

1004 Guenet, B., Moyano, F. E., Peylin, P., Ciais, P. and Janssens, I. A.: Towards a representation
1005 of priming on soil carbon decomposition in the global land biosphere model ORCHIDEE
1006 (version 1.9.5.2), *Geosci. Model Dev.*, 9, 841–855, 2016.

1007 Haile, S. G., Nair, V. D. and Nair, P. K. R.: Contribution of trees to carbon storage in soils of
1008 silvopastoral systems in Florida, USA, *Glob. Chang. Biol.*, 16, 427–438, 2010.

1009 Hendrick, R. L. and Pregitzer, K. S.: Temporal and depth-related patterns of fine root dynamics
1010 in northern hardwood forests, *J. Ecol.*, 84, 167–176, 1996.

1011 Howlett, D. S., Moreno, G., Mosquera Losada, M. R., Nair, P. K. R. and Nair, V. D.: Soil
1012 carbon storage as influenced by tree cover in the Dehesa cork oak silvopasture of central-
1013 western Spain, *J. Environ. Monit.*, 13(7), 1897–904, 2011.

1014 Ilstedt, U., Bargués Tobella, A., Bazié, H. R., Bayala, J., Verbeeten, E., Nyberg, G., Sanou, J.,
1015 Benegas, L., Murdiyarso, D., Laudon, H., Sheil, D. and Malmer, A.: Intermediate tree cover

1016 can maximize groundwater recharge in the seasonally dry tropics, *Sci. Rep.*, 6, 21930, 2016.

1017 IUSS Working Group WRB: World Reference Base for Soil Resources 2006, first update 2007.

1018 World Soil Resources Reports No. 103. FAO, Rome., 2007.

1019 Jobbagy, E. G. and Jackson, R. B.: The vertical distribution of soil organic carbon and its
1020 relation to climate and vegetation, *Ecol. Appl.*, 10, 423–436, 2000.

1021 Joslin, J. D., Gaudinski, J. B., Torn, M. S., Riley, W. J. and Hanson, P. J.: Fine-root turnover
1022 patterns and their relationship to root diameter and soil depth in a ¹⁴C-labeled hardwood forest,
1023 *New Phytol.*, 172, 523–535, 2006.

1024 Kätterer, T., Bolinder, M. A., Andrén, O., Kirchmann, H. and Menichetti, L.: Roots contribute
1025 more to refractory soil organic matter than above-ground crop residues, as revealed by a long-
1026 term field experiment, *Agric. Ecosyst. Environ.*, 141, 184–192, 2011.

1027 Keiluweit, M., Bougoure, J. J., Nico, P. S., Pett-Ridge, J., Weber, P. K. and Kleber, M.: Mineral
1028 protection of soil carbon counteracted by root exudates, *Nat. Clim. Chang.*, 5, 588–595, 2015.

1029 Kim, D.-G., Kirschbaum, M. U. F. and Beedy, T. L.: Carbon sequestration and net emissions
1030 of CH₄ and N₂O under agroforestry: Synthesizing available data and suggestions for future
1031 studies, *Agric. Ecosyst. Environ.*, 226, 65–78, 2016.

1032 Koarashi, J., Hockaday, W. C., Masiello, C. A. and Trumbore, S. E.: Dynamics of decadal
1033 cycling carbon in subsurface soils, *J. Geophys. Res.*, 117, 1–13, 2012.

1034 Koven, C. D., Riley, W. J., Subin, Z. M., Tang, J. Y., Torn, M. S., Collins, W. D., Bonan, G.
1035 B., Lawrence, D. M. and Swenson, S. C.: The effect of vertically resolved soil biogeochemistry
1036 and alternate soil C and N models on C dynamics of CLM4, *Biogeosciences*, 10(11), 7109–
1037 7131, 2013.

1038 Lange, M., Eisenhauer, N., Sierra, C. A., Bessler, H., Engels, C., Griffiths, R. I., Mellado-
1039 Vázquez, P. G., Malik, A. A., Roy, J., Scheu, S., Steinbeiss, S., Thomson, B. C., Trumbore, S.

1040 E. and Gleixner, G.: Plant diversity increases soil microbial activity and soil carbon storage,
1041 *Nat. Commun.*, 6, 6707, 2015.

1042 Lavelle, P.: Faunal activities and soil processes: adaptative strategy that determine ecosystem
1043 function., 1997.

1044 Li, F., Meng, P., Fu, D. and Wang, B.: Light distribution, photosynthetic rate and yield in a
1045 *Paulownia-wheat intercropping system in China*, *Agrofor. Syst.*, 74(2), 163–172, 2008.

1046 Lorenz, K. and Lal, R.: Soil organic carbon sequestration in agroforestry systems. A review,
1047 *Agron. Sustain. Dev.*, 34, 443–454, 2014.

1048 Luedeling, E., Smethurst, P. J., Baudron, F., Bayala, J., Huth, N. I., van Noordwijk, M., Ong,
1049 C. K., Mulia, R., Lusiana, B., Muthuri, C. and Sinclair, F. L.: Field-scale modeling of tree-crop
1050 interactions: Challenges and development needs, *Agric. Syst.*, 142, 51–69, 2016.

1051 Mead, R. and Willey, R. W.: The concept of a “land equivalent ratio” and advantages in yields
1052 from intercropping, *Exp. Agric.*, 16(3), 217–228, 1980.

1053 Moreno, G., Obrador, J. J., Cubera, E. and Dupraz, C.: Fine root distribution in Dehesas of
1054 central-western Spain, *Plant Soil*, 277(1–2), 153–162, 2005.

1055 Moyano, F. E., Vasilyeva, N., Bouckaert, L., Cook, F., Craine, J., Curiel Yuste, J., Don, A.,
1056 Epron, D., Formanek, P., Franzluebbers, A., Ilstedt, U., Kätterer, T., Orchard, V., Reichstein,
1057 M., Rey, A., Ruamps, L., Subke, J. A., Thomsen, I. K. and Chenu, C.: The moisture response
1058 of soil heterotrophic respiration: Interaction with soil properties, *Biogeosciences*, 9, 1173–
1059 1182, 2012.

1060 Moyano, F. E., Manzoni, S. and Chenu, C.: Responses of soil heterotrophic respiration to
1061 moisture availability: An exploration of processes and models, *Soil Biol. Biochem.*, 59, 72–85,
1062 2013.

1063 Mulia, R. and Dupraz, C.: Unusual fine root distributions of two deciduous tree species in

1064 southern France: What consequences for modelling of tree root dynamics?, *Plant Soil*, 281, 71–
1065 85, 2006.

1066 Mulia, R., Dupraz, C. and van Noordwijk, M.: Reconciling root plasticity and architectural
1067 ground rules in tree root growth models with voxel automata, *Plant Soil*, 337(1–2), 77–92, 2010.

1068 Nair, P. K.: *An introduction to agroforestry*, Kluwer Academic Publishers, Dordrecht, The
1069 Netherlands., 1993.

1070 Nair, P. K. R.: Classification of agroforestry systems, *Agrofor. Syst.*, 3(2), 97–128, 1985.

1071 van Noordwijk, M. and Lusiana, B.: WaNuLCAS, a model of water, nutrient and light capture
1072 in agroforestry systems, *Agrofor. Syst.*, 43, 217–242, 1999.

1073 Odhiambo, H. O., Ong, C. K., Deans, J. D., Wilson, J., Khan, A. A. H. and Sprent, J. I.: Roots,
1074 soil water and crop yield: Tree crop interactions in a semi-arid agroforestry system in Kenya,
1075 *Plant Soil*, 235(2), 221–233, 2001.

1076 Oelbermann, M. and Voroney, R. P.: An evaluation of the century model to predict soil
1077 organic carbon: examples from Costa Rica and Canada, *Agrofor. Syst.*, 82, 37–50, 2011.

1078 Oelbermann, M., Voroney, R. P. and Gordon, A. M.: Carbon sequestration in tropical and
1079 temperate agroforestry systems: a review with examples from Costa Rica and southern Canada,
1080 *Agric. Ecosyst. Environ.*, 104, 359–377, 2004.

1081 Oelbermann, M., Voroney, R. P., Thevathasan, N. V., Gordon, A. M., Kass, D. C. L. and
1082 Schlönvoigt, A. M.: Soil carbon dynamics and residue stabilization in a Costa Rican and
1083 southern Canadian alley cropping system, *Agrofor. Syst.*, 68(1), 27–36, 2006.

1084 Ong, C. K. and Leakey, R. R. B.: Why tree-crop interactions in agroforestry appear at odds with
1085 tree-grass interactions in tropical savannahs, *Agrofor. Syst.*, 45(1–3), 109–129, 1999.

1086 Parton, W. J., Schimel, D. S., Cole, C. V and Ojima, D. S.: Analysis of factors controlling soil
1087 organic matter levels in great plains grasslands, *Soil Sci. Soc. Am. J.*, 51, 1173–1179, 1987.

1088 Peichl, M., Thevathasan, N. V, Gordon, A. M., Huss, J. and Abohassan, R. A.: Carbon
1089 sequestration potentials in temperate tree-based intercropping systems, southern Ontario,
1090 Canada, *Agrofor. Syst.*, 66, 243–257, 2006.

1091 Perveen, N., Barot, S., Alvarez, G., Klumpp, K., Martin, R., Rapaport, A., Herfurth, D.,
1092 Louault, F. and Fontaine, S.: Priming effect and microbial diversity in ecosystem functioning
1093 and response to global change: A modeling approach using the SYMPHONY model, *Glob.*
1094 *Chang. Biol.*, 20(4), 1174–1190, 2014.

1095 Price, G. W. and Gordon, A. M.: Spatial and temporal distribution of earthworms in a temperate
1096 intercropping system in southern Ontario, Canada, *Agrofor. Syst.*, 44, 141–149, 1999.

1097 Prieto, I., Roumet, C., Cardinael, R., Kim, J., Maeght, J.-L., Mao, Z., Portillo, N.,
1098 Thammahacksa, C., Dupraz, C., Jourdan, C., Pierret, A., Roupsard, O. and Stokes, A.: Root
1099 functional parameters along a land-use gradient: evidence of a community-level economics
1100 spectrum, *J. Ecol.*, 103, 361–373, 2015.

1101 Prieto, I., Stokes, A. and Roumet, C.: Root functional parameters predict fine root
1102 decomposability at the community level, *J. Ecol.*, 104, 725–733, 2016.

1103 R Development Core Team: *R: A language and environment for statistical computing*, 2013.

1104 Rasse, D. P., Mulder, J., Moni, C. and Chenu, C.: Carbon turnover kinetics with depth in a
1105 French loamy soil, *Soil Sci. Soc. Am. J.*, 70, 2097–2105, 2006.

1106 Salomé, C., Nunan, N., Pouteau, V., Lerch, T. Z. and Chenu, C.: Carbon dynamics in topsoil
1107 and in subsoil may be controlled by different regulatory mechanisms, *Glob. Chang. Biol.*, 16,
1108 416–426, 2010.

1109 Santaren, D., Peylin, P., Viovy, N. and Ciais, P.: Optimizing a process-based ecosystem model
1110 with eddy-covariance flux measurements: A pine forest in southern France, *Global*
1111 *Biogeochem. Cycles*, 21, 1–15, 2007.

1112 Schwarz, G.: Estimating dimension of a model, *Ann. Stat.*, 6(2), 461–464, 1978.

1113 Shahzad, T., Chenu, C., Genet, P., Barot, S., Perveen, N., Mougin, C. and Fontaine, S.:
1114 Contribution of exudates, arbuscular mycorrhizal fungi and litter depositions to the rhizosphere
1115 priming effect induced by grassland species, *Soil Biol. Biochem.*, 80, 146–155, 2015.

1116 Sierra, C. A., Trumbore, S. E., Davidson, E. A., Vicca, S. and Janssens, I.: Sensitivity of
1117 decomposition rates of soil organic matter with respect to simultaneous changes in temperature
1118 and moisture, *J. Adv. Model. Earth Syst.*, 7, 335–356, 2015.

1119 Soetaert, K., Petzoldt, T. and Woodrow Setzer, R.: Solving Differential Equations in R:
1120 Package deSolve, *J. Stat. Softw.*, 33(9), 1–25, 2010.

1121 Somarriba, E.: Revisiting the past: an essay on agroforestry definition, *Agrofor. Syst.*, 19(3),
1122 233–240, 1992.

1123 Steinbeiss, S., Beßler, H., Engels, C., Temperton, V. M., Buchmann, N., Roscher, C.,
1124 Kreuziger, Y., Baade, J., Habekost, M. and Gleixner, G.: Plant diversity positively affects
1125 short-term soil carbon storage in experimental grasslands, *Glob. Chang. Biol.*, 14(12), 2937–
1126 2949, 2008.

1127 Sulman, B. N., Phillips, R. P., Oishi, A. C., Shevliakova, E. and Pacala, S. W.: Microbe-driven
1128 turnover offsets mineral-mediated storage of soil carbon under elevated CO₂, *Nat. Clim.*
1129 *Chang.*, 4, 1099–1102, 2014.

1130 Taghizadeh-Toosi, A., Christensen, B. T., Hutchings, N. J., Vejlin, J., Kätterer, T., Glendining,
1131 M. and Olesen, J. E.: C-TOOL: A simple model for simulating whole-profile carbon storage in
1132 temperate agricultural soils, *Ecol. Modell.*, 292, 11–25, 2014.

1133 Talbot, G.: L'intégration spatiale et temporelle du partage des ressources dans un système
1134 agroforestier noyers-céréales: une clef pour en comprendre la productivité ?, PhD Dissertation,
1135 Université Montpellier II., 2011.

1136 Tarantola, A.: Inverse problem theory: methods for data fitting and model parameter estimation,
1137 edited by Elsevier., 1987.

1138 Tarantola, A.: Inverse Problem Theory and Methods for Model Parameter Estimation, edited
1139 by SIAM., 2005.

1140 Thevathasan, N. V. and Gordon, A. M.: Poplar leaf biomass distribution and nitrogen dynamics
1141 in a poplar-barley intercropped system in southern Ontario, Canada, *Agrofor. Syst.*, 37, 79–90,
1142 1997.

1143 Udawatta, R. P., Kremer, R. J., Adamson, B. W. and Anderson, S. H.: Variations in soil
1144 aggregate stability and enzyme activities in a temperate agroforestry practice, *Appl. Soil Ecol.*,
1145 39(2), 153–160, 2008.

1146 Virto, I., Barré, P., Burlot, A. and Chenu, C.: Carbon input differences as the main factor
1147 explaining the variability in soil organic C storage in no-tilled compared to inversion tilled
1148 agrosystems, *Biogeochemistry*, 108, 17–26, 2012.

1149 van der Werf, W., Keesman, K., Burgess, P., Graves, A., Pilbeam, D., Incoll, L. D., Metselaar,
1150 K., Mayus, M., Stappers, R., van Keulen, H., Palma, J. and Dupraz, C.: Yield-SAFE: A
1151 parameter-sparse, process-based dynamic model for predicting resource capture, growth, and
1152 production in agroforestry systems, *Ecol. Eng.*, 29(4), 419–433, 2007.

1153 Wutzler, T. and Reichstein, M.: Colimitation of decomposition by substrate and decomposers
1154 - a comparison of model formulations, *Biogeosciences*, 5, 749–759, 2008.

1155 Wutzler, T. and Reichstein, M.: Priming and substrate quality interactions in soil organic matter
1156 models, *Biogeosciences*, 10(3), 2089–2103, 2013.

1157 Yin, R. and He, Q.: The spatial and temporal effects of paulownia intercropping: The case of
1158 northern China, *Agrofor. Syst.*, 37, 91–109, 1997.

1159 Zhang, W., Wang, X. and Wang, S.: Addition of external organic carbon and native soil organic

1160 carbon decomposition: a meta-analysis., PLoS One, 8(2), e54779, 2013.

1161

1162

1163

1164

1165

1166

1167

1168

1169

1170

1171

1172

1173

1174

1175

1176